https://doi.org/10.5194/esd-2024-29
Preprint. Discussion started: 28 August 2024

Earth System Dynamics Discussions
Open Access
EGU

Estimating lateral nitrogen transfer through the global river network using a land surface model

Minna Ma[1*], Haicheng Zhang[2*], Ronny Lauerwald[3], Philippe Ciais[4], Pierre Regnier[1]

[1] Department Geoscience, Environment & Society-BGEOSYS, Université libre de Bruxelles, 1050 Bruxelles, Belgium

[2] School of Geography and Planning, Sun Yat-sen University, Guangzhou, Guangdong, 510006, China

[3] Université Paris-Saclay, INRAE, AgroParisTech, UMR ECOSYS, Palaiseau, France

[4] Laboratoire des Sciences du Climat et de l' Environnement, IPSL-LSCE CEA/CNRS/UVSQ, Orme des Merisiers, 91191, Gif sur Yvette, France

Correspondence: Minna Ma (minna.ma@ulb.be) and Haicheng Zhang (zhanghch59@mail.sysu.edu.cn).

https://doi.org/10.5194/esd-2024-29
Preprint. Discussion started: 28 August 2024


Earth System Dynamics
Discussions
Open Access
EGU

Abstract. Lateral nitrogen (N) transport from land to oceans through rivers is an important component of the global N cycle. We developed a new model of this system, called ORCHIDEE-NLAT, which simulates the routing of water in rivers, and the pertaining transport of dissolved inorganic N (DIN), dissolved organic N (DON) and particulate organic N (PON) as well as the accompanying biogeochemical processes of decomposition for DON and PON, and denitrification for DIN during the transit from land to oceans through the river network. Evaluation against global observation-based datasets reveal that the model captures both the magnitude and seasonal variations of riverine water discharges and total nitrogen (TN) flows well. The ORCHIDEE-NLAT model was then applied to reconstruct the historical evolution of global TN flows from land to rivers, as well as the denitrification of DIN within the river network. Due to anthropogenic activities (e.g. mineral fertilisers and manure application, sewage water injection in rivers and land use change) and indirect climate and CO_2 effects, the TN exports are modelled to increase from 27.1 Tg N yr^{-1} over 1901-1910 to 40.8 Tg N yr^{-1} over 2001-2014, with DIN (80%) contributing most of this increase. The annual mean TN flow and DIN denitrification rates show substantial spatial heterogeneities. The seasonal amplitude of TN flow is of similar magnitude as the large-scale spatial variability. Compared to previously published global aquatic N transfer models (IMAGE-GNM, FrAMES-N, MBM, DLEM and Global NEWS2), our model produces similar global and continental-scale TN exports to the ocean, but shows distinct patterns at finer scale spatial scales (e.g. basin scale). ORCHIDEE-NLAT could also be coupled with other land surface models such as those used in the Nitrogen Model Intercomparison Project (NMIP). Our model provides a full simulation of N transport and reactivity from soils to oceans at an unprecedented spatio-temporal resolution (daily fluxes at 0.5° globally).

1. Introduction

https://doi.org/10.5194/esd-2024-29
Preprint. Discussion started: 28 August 2024


Earth System Dynamics Discussions Open Access EGU

Nitrogen (N) is an essential element for all life on Earth, and the N cycle interacts in multiple ways with the Earths climate system and the environment. Nitrous oxide (N_2O) is an important greenhouse gas, which affects Earths energy balance in a similar way as carbon dioxide (CO_2) but is nearly 300 times more effective on a per molecule basis (Sainju et al., 2014). N also affects the C cycling, CO_2 and methane (CH_4) fluxes as it limits primary production rates in many terrestrial, freshwater and marine ecosystems (Thornton et al., 2007; Moore et al., 2013; Zaehle et al., 2014; Seiler et al., 2024). The N cycle thus plays an important role in controlling the C cycle and climate change, which calls for an analysis of the N dynamics in the context of changing C cycle, climate and anthropogenic activities. In this Earth system perspective, insufficient attention has been given to the tight link between the terrestrial and marine N cycles through the Land to Ocean Aquatic Continuum (LOAC) (Galloway et al., 2003; Billen et al., 2013; Maranger et al., 2018). Existing studies have largely treated the land and open ocean cycles separately, ignoring N processes occurring along the LOAC (Fowler et al., 2013; Zhang et al., 2021). The representation of N processes in the LOAC is required to achieve a dynamic coupling between land surface and ocean biogeochemical models, with land surface models simulating the dynamically changing N exports to the coast, which may include historical hindcasts and future projections.

Over the past several decades, the cumulative effects of climate change, increased population, industrialization and agricultural fertiliser use have accelerated the global N cycle, and increased N leaching into the LOAC (Bouwman et al., 2005; Kim et al., 2011; Swaney et al., 2012; Beusen et al., 2016). This has resulted in negative human health and environmental impacts such as drinking water degradation and an increase in frequency and severity of eutrophication (Dodds & Smith, 2016; Huang et al., 2017; Costa et al., 2018; Lee et al., 2019; Dai et al., 2023). Most land surface models include N leaching

https://doi.org/10.5194/esd-2024-29
Preprint. Discussion started: 28 August 2024

to aquatic systems, this process is rarely evaluated in quantitative terms using observations collected within the fluvial network. It has been shown that N leaching is inaccurate in most LSMs (Feng et al., 2023), which in turn affects the simulation of the response of terrestrial C and N cycles to anthropogenic activities and climate change (Thomas et al., 2013). Furthermore, explicit representation of the fate of the land-derived N inputs into the LOAC is required to better constrain the response of the ocean C cycle to increased nutrient inputs (Lacroix et al., 2021; Resplandy et al., 2024) as well as to assess the extent to which N pollution reduction scenarios can mitigate (Satter et al., 2014) eutrophication in riverine and coastal aquatic ecosystems (Hashemi et al., 2016; Desmit et al., 2018).

The representation of N lateral transfers through aquatic systems is challenging because it requires to represent multiple N sources, transformation, transport, and retention processes along the global fluvial network. A variety of models with different structures and representations of the water and N cycles have been developed (Luscz et al., 2015, 2017). Models such as SWAT (the Soil and Water Assessment Tool) (Arnold et al., 1998; Liu et al., 2017), HSPF (the Hydrologic Simulation Program-FORTRAN) (Bicknell et al., 2005; Wang et al., 2015) and HYPE (HYdrological Predictions for the Environment) (Lindstrom et al., 2010; Donnelly et al., 2014) represent hydrology and N transport and transformation processes in rivers, but mainly for catchment scale applications. Therefore, their complexity and high data requirements for calibration and evaluation limit their applicability, in particular the long-term evolution of global N fluxes and transformation processes. Simplified empirical approaches provide an alternative for large-scale simulations, such as the Global NEWS2 model (Global Nutrient Export from Watersheds 2) allowing to estimate riverine N exports to the ocean as a function of N deliveries from the surrounding catchment with a highly simplified representation of N transport

https://doi.org/10.5194/esd-2024-29
Preprint. Discussion started: 28 August 2024


Earth System Dynamics Discussions Open Access EGU

and in-stream N processes (Seitzinger et al., 2005; Mayorga et al., 2010; Lee et al., 2016). The Integrated Model to Assess the Global Environment-Global Nutrient Model (IMAGE-GNM) provides a more process-based representation of the river network as it relies on a globally distributed, spatially explicit hydrological model (PCR-GLOBWB, PCR aster Global Water Balance) to estimate N delivery to surface waters and its subsequent transport (Beusen et al. 2014, 2016 & 2022; Vilmin et al., 2018). This model however simulates N retention according to empirical formulas, is not dynamically coupled to vegetation-soil N processes and only provides yearly averaged fluxes, hence ignoring the seasonal fluctuations induced by the hydrology and N cycling on land and in the river network. The Dynamic Land Ecosystem Model (DLEM 2.0) was improved to simulate riverine N flow from terrestrial ecosystems to rivers and coastal oceans. So far, however, the N lateral transfer simulated by DLEM has only been evaluated at regional scale (eastern North America, Yang et al., 2015) or for N_2O emissions on the global scale (Tian et al. 2018; Yao et al., 2020). To complement these studies, we develop a new N lateral transfer model that can be linked to the outputs of land surface models while capturing the hydrology and N transformation processes in the global river network at a temporal resolution (days to months) as relevant for biogeochemical processes in coastal and marine ecosystems. At the same time, this model should be able to reconstruct and forecast the long-term (decadal to century-scale) evolution of the aquatic N cycle as a result of a wide variety of anthropogenic factors, including climate change.

Our model is an offline model of lateral N transfers which is fed with outputs from the land surface model ORCHIDEE. ORCHIDEE is a widely used land-surface model (Krinner et al., 2005), with many versions (or branches) focusing on different aspects of the terrestrial C cycle and associated bio-elements. We leverage ORCHIDEE-CNP, the branch simulating the coupled

https://doi.org/10.5194/esd-2024-29
Preprint. Discussion started: 28 August 2024


Earth System Dynamics Discussions Open Access EGU

cycles of carbon (C), N and phosphorus (P) in the terrestrial biosphere (Sun et al., 2021), and ORCHIDEE-Clateral, the branch simulating the leaching and erosion of C along the soil-inland water continuum (Lauerwald et al., 2017; Lauerwald et al., 2020; Zhang et al., 2022). Our study is structured as follows: (1) development of an offline N lateral transfer model (ORCHIDEE-NLAT) driven by output from ORCHIDEE-Clateral and ORCHIDEE-CNP; (2) collection of observations of water discharge and N concentration to evaluate the performance of ORCHIDEE-NLAT; (3) investigation of the spatio-temporal dynamics of N lateral transfer over the historical period (1900-2014); and (4) comparison of model results with those obtained with previously published models.

2. Methods and Data

2.1. Model development

2.1.1. The ORCHIDEE-NLAT model

The ORCHIDEE land surface model comprehensively simulates the cycling of energy, water and C, in terrestrial ecosystems (Krinner et al., 2005). As the model evolved, many versions (or branches) emerged with various foci on additional land surface processes impacting the climate system. In particular, the ORCHIDEE-CNP branch features a detailed representation of the coupled cycling of C, N, and P in vegetation and soil (e.g. root uptake of N, the allocation of N in the tissue of different parts of vegetation biomass, N turnover in litter and soil organic matter) and the leaching of NH_4^+ and NO_3^- from soils to inland waters (Goll et al., 2017, 2018; Sun et al., 2021). The ORCHIDEE-Clateral branch stimulates the large-scale lateral transfer and fate of water, sediment, particulate (POC) and dissolved organic C (DOC), and CO_2 along the land-river-ocean continuum (Lauerwald et al., 2017; Zhang et al., 2020, 2022).

https://doi.org/10.5194/esd-2024-29
Preprint. Discussion started: 28 August 2024

Based on the land-to-river inputs of water, POC, DOC and inorganic N simulated by ORCHIDEE-CNP and ORCHIDEE-Clateral, we developed the ORCHIDEE-NLAT model to simulate the transfers of reactive N through the global river network. We use an offline approach which has the advantage of running fast, and the potential to be coupled with output from other LSMs. In this offline approach, ORCHIDEE-CNP provides as input the leaching rates of terrestrial dissolved inorganic N (DIN) with surface runoff and subsoil drainage and dissolved organic N (DON) leaching from manure. Inputs of terrestrial DON and particulate organic N (PON) are derived from the leaching and erosional fluxes of DOC and POC simulated by ORCHIDEE-Clateral and stoichiometric C:N ratios of dissolved organic matter (DOM) and particulate organic matter (POM), please refer to section 2.1.2 for details (Fig. 1).

During the twentieth century, global N (DIN and DON) discharge to surface water from sewage increased about 3.5-fold to 7.7 Tg N yr^{-1}, which has large impact on the global N lateral transfer. N discharge from sewage also included in ORCHIDEE-NLAT using N sewage dataset (1900-2010, gridded maps every five years) reported by Beusen et al. (2016). N in sewage comes from three kinds of sources: human waste from urban environments, animal waste, and industrial waste, which has different fates, please read details in Van Drecht (2009) and Morée et al (2013).

PON, DON and DIN are transported by advection with the flow of water: from soils to rivers and through the river network all the way to the coast. Within the river network, part of the transported DON and PON is decomposed to DIN, and part of DIN is released back to the atmosphere through denitrification processes. Following previous global modelling approaches (Aitkenhead-Peterson et al., 2001; Bernot and Dodds, 2005; Wollheim et al., 2008), ORCHIDEE-NLAT simulates DIN denitrification without explicit

https://doi.org/10.5194/esd-2024-29
Preprint. Discussion started: 28 August 2024

Earth System Dynamics
Discussions
Open Access
EGU

representation of the different DIN species (i.e. NO_3^- and NH_4^+) or their interconversion via nitrification (Fig.1).

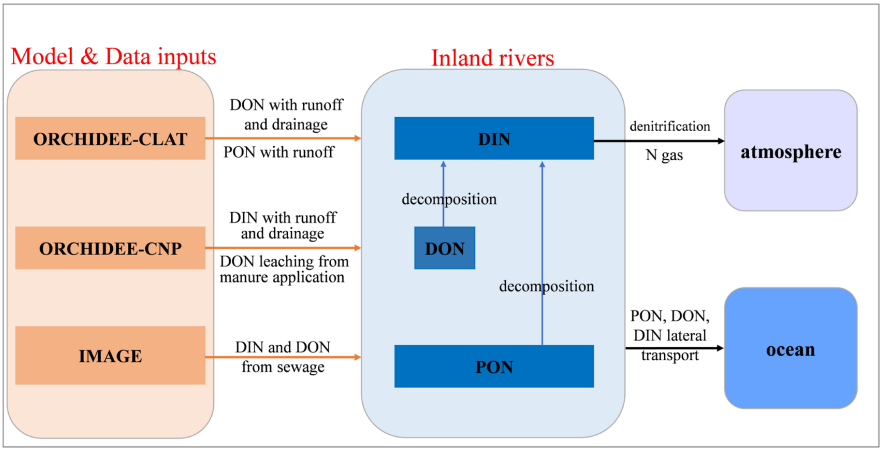

Figure 1. Sources of themodel driving data and the main aquatic N transformation processes in ORCHIDEE-NLAT.

2.1.2. N delivery from upland soils to the river network

The lateral transfer of DOC and POC from land to rivers was used to constrain DON and PON inputs. PON erosion with runoff originates from three soil organic matter (SOM) pools characterised by different C:N ratios set to 12, 25 and 8 for active, slow and passive SOM pools, respectively (Zhang et al., 2022). The PON erosion from each pool is calculated by dividing the POC erosion flux from the same SOM pool by its corresponding C:N ratio. For DON leaching with runoff and drainage, we relied on measurements of the stoichiometry of dissolved organic matter, which report C:N ratios in soil and rivers comprised between 8 and 25, with an average value of around 12 (Kirkby et al., 2011; Lutz et al., 2011; Tipping et al., 2016; Maranger et al., 2018; Rodríguez-Cardona et al., 2021). Therefore, the leaching of DON with runoff and drainage were quantified from ORCHIDEE-Clateral simulations of the corresponding DOC fluxes and an average C:N ratio of 12, noting that the resulting flow excludes the DON leaching caused by manure application (this

https://doi.org/10.5194/esd-2024-29
Preprint. Discussion started: 28 August 2024


Earth System Dynamics Discussions Open Access EGU

source is not accounted for in ORCHIDEE-Clateral). The spatial and temporal resolution of the resulting DON and PON flow used to force ORCHIDEE-NLAT was 1° with a timestep of one day (Table 1) and these inputs were resampled to the nominal resolution of ORCHIDEE-NLAT of 0.5° using the nearest-neighbour resampling (Patil, 2018).

DIN (i.e. NH_4^+ and NO_3^-) inputs from soils to rivers was prescribed from a simulation of ORCHIDEE-CNP (Goll et al., 2017a, 2018; Sun et al., 2021) which include DIN leaching from natural and cultivated (e.g. cropland and pasture) ecosystems, and account for changes induced by atmospheric N deposition, fertiliser use and manure application. DON inputs to rivers from manure application were prescribed from ORCHIDEE-CNP based on a DON pool and leaching factor, a separate DON pool from manure being added into ORCHIDEE-CNP to participate in the subsequent N cycling and leaching processes. The spatial and temporal resolution of this input dataset was 2° with a daily time step and were downscaled to the ORCHIDEE-NLAT spatial resolution of 0.5° using the nearest-neighbour resampling (Patil, 2018) (Table 1).

Finally, the N inputs from sewage (https://doi.org/10.17026/dans-zgs-9k9m) provided at 0.5° globally but with a yearly timestep (Beusen et al, 2016) were redistributed evenly across each day of the year (Table 1).

2.1.3. N transport and transformation in the river network

ORCHIDEE-NLAT simulates river discharge along a distributed routing scheme (Vörösmarty et al., 2000). As shown in Fig. 2, surface runoff (F_{RO}) and belowground drainage (F_{DR}), both as model inputs extracted from ORCHIDEE-Clateral, first feed into the "fast" (S_{fast_H2O}, m^3) and "slow" water reservoirs (S_{slow_H2O}, m^3), respectively. The delayed outflows from these reservoirs then feed into the "stream" water reservoir (S_{stream_H2O}, m^3). The outflow rates from

https://doi.org/10.5194/esd-2024-29
Preprint. Discussion started: 28 August 2024

Earth System Dynamics
Discussions
Open Access
EGU

the fast ($F_{fastout\_H2O}$, $m^3\ d^{-1}$) and slow ($F_{slowout\_H2O}$, $m^3\ d^{-1}$) reservoirs are calculated at a daily time-step based on a grid-cell-specific topographic index f_{topo} (unitless, Vörösmarty et al., 2000) (Table 1) and a reservoir-specific water turnover factor τ, which translates f_{topo} into a water residence time for each reservoir attached to each river segment (Eqs. 1 and 2). Water in the stream reservoir (S_{stream_H2O}) in grid cell i then flows downstream (Eq. 3) into the stream reservoir of grid cell $i+1$ ($F_{downstream\_H2O}$, $m^3\ d^{-1}$). The τ_{fast}, τ_{slow} and τ_{stream} are set to 3.0 days, 25.0 days and 0.24 days, which are default settings in ORCHIDEE (Ngo-Duc et al., 2006).

$$F_{fastout\_H2O} = \frac{S_{fast\_H2O}}{\tau_{fast} \times f_{topo}} \quad (1)$$

$$F_{slowout\_H2O} = \frac{S_{slow\_H2O}}{\tau_{slow} \times f_{topo}} \quad (2)$$

$$F_{downstream\_H2O} = \frac{S_{stream\_H2O}}{\tau_{stream} \times f_{topo}} \quad (3)$$

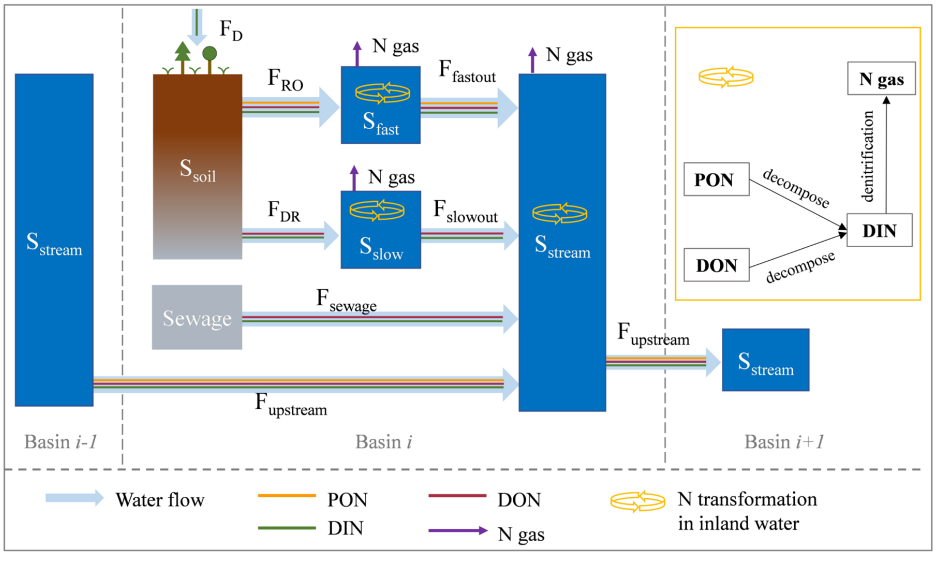

Figure 2. Schematic plot for the reservoirs and flows of water and N in ORCHIDEE-NLAT. S_{soil} is the soil pool. S_{fast}, S_{slow}, S_{stream} are the "fast", "slow" and stream reservoir, respectively. F_{RO} and F_{DR} are surface runoff and belowground drainage, respectively. $F_{fastout}$ is the flow from fast reservoir to stream reservoir. $F_{slowout}$ is the flow from slow reservoir to stream reservoir.

https://doi.org/10.5194/esd-2024-29
Preprint. Discussion started: 28 August 2024


Earth System Dynamics
Discussions
Open Access
EGU

$F_{upstream}$ and $F_{downstream}$ are the upstream inputs from basin *i-1* and downstream outputs to basin *i+1*, respectively. F_D is the wet and dry deposition of DIN from the atmosphere.

Following the routing scheme of water in ORCHIDEE-NLAT, N contained in surface runoff (F_{RO}) and belowground drainage (F_{DR}) flows into the fast and slow reservoir, respectively. Subsequently, and depending on the water residence time, the N stocks in these reservoirs are subject to decomposition and losses via denitrification. The remaining fractions flow further into the stream reservoirs, which also receive N inputs delivered directly by sewage (Fig. 2). Within stream reservoirs, N is transformed by biogeochemical reactions and flows from grid cell to grid cell along the river routing scheme. The timescale for biogeochemical transformation processes scale to the water residence time (and hence topography) within the river network, and the fraction of N that is not lost to the atmosphere via denitrification is ultimately exported to the coast. The biogeochemical reactions within each reservoir include the decomposition of PON and DON to DIN, and the denitrification of DIN to N gas which is assumed all released to the atmosphere (Fig. 2). The mass balance equations for the N stocks in different reservoirs are calculated as follows:

$$\frac{dS_{fast\_PON}}{dt} = F_{RO\_PON} - F_{fastout\_PON} - R_{fast\_PON} \quad (4)$$

$$\frac{dS_{fast\_DON}}{dt} = F_{RO\_DON} - F_{fastout\_DON} - R_{fast\_DON} \quad (5)$$

$$\frac{dS_{fast\_DIN}}{dt} = F_{RO\_DIN} - F_{fastout\_DIN} - R_{fast\_DIN} \quad (6)$$

$$\frac{dS_{slow\_DON}}{dt} = F_{DR\_DON} - F_{slowout\_DON} - R_{slow\_DON} \quad (7)$$

$$\frac{dS_{slow\_DIN}}{dt} = F_{DR\_DIN} - F_{slowout\_DIN} - R_{slow\_DIN} \quad (8)$$

https://doi.org/10.5194/esd-2024-29
Preprint. Discussion started: 28 August 2024


Earth System Dynamics
Discussions
Open Access
EGU

$$\frac{dS_{stream\_PON}}{dt} = F_{fastout\_PON} + F_{upstream\_PON} - R_{stream\_PON} - F_{downstream\_PON} \quad (9)$$

$$\frac{dS_{stream\_DON}}{dt} = F_{fastout\_DON} + F_{slowout\_DON} + F_{upstream\_DON} + F_{sewage\_DON} - R_{stream\_DON} - R_{downstream\_DON} \quad (10)$$

$$\frac{dS_{stream\_DIN}}{dt} = F_{fastout\_DIN} + F_{slowout\_DIN} + F_{upstream\_DIN} + F_{sewage\_DIN} + R_{stream\_PON} + R_{stream\_DON} - R_{stream\_DIN} - F_{downstream\_DIN} \quad (11)$$

where $F_{upstream\_PON}$ (g N d^{-1}), $F_{upstream\_DON}$ (g N d^{-1}) and $F_{upstream\_DIN}$ (g N d^{-1}) represent the inflow rates of PON, DON and DIN, respectively, from upstream grids to the next grid; $F_{downstream\_PON}$ (g N d^{-1}), $F_{downstream\_DON}$ (g N d^{-1}) and $F_{downstream\_DIN}$ (g N d^{-1}) represent outflow rates of PON, DON and DIN from a given grid to downstream grid, respectively. For each N species, the N inputs to a stream reservoir in a given grid cell *i* ($F_{upstream\_PON}$, $F_{upstream\_DON}$ and $F_{upstream\_DON}$ in Eqs. 9-11) is equal to the N outflow from the upstream stream reservoir in the grid cell *i-1* ($F_{streamdown\_PON}$, $F_{streamdown\_PON}$ and $F_{streamdown\_PON}$ in Eqs. 17-19).

We assume that N concentrations are homogeneously distributed within each reservoir of each grid and that the transfers of N from one reservoir to another simply follow that of water. N transfers are calculated according to:

$$F_{fastout\_PON} = S_{fast\_PON} \times \frac{F_{fastout\_H2O}}{S_{fast\_H2O}} \quad (12)$$

$$F_{fastout\_DON} = S_{fast\_DON} \times \frac{F_{fastout\_H2O}}{S_{fast\_H2O}} \quad (13)$$

$$F_{fastout\_DIN} = S_{fast\_DIN} \times \frac{F_{fastout\_H2O}}{S_{fast\_H2O}} \quad (14)$$

$$F_{slowout\_DON} = S_{slow\_DON} \times \frac{F_{slowout\_H2O}}{S_{slow\_H2O}} \quad (15)$$

$$F_{slowout\_DIN} = S_{slow\_DIN} \times \frac{F_{slowout\_H2O}}{S_{slow\_H2O}} \quad (16)$$

https://doi.org/10.5194/esd-2024-29
Preprint. Discussion started: 28 August 2024

Earth System Dynamics
Discussions
Open Access
EGU

$$F_{streamdown\_PON} = S_{stream\_PON} \times \frac{F_{streamout\_H2O}}{S_{stream\_H2O}} \quad (17)$$

$$F_{streamdown\_DON} = S_{stream\_DON} \times \frac{F_{streamout\_H2O}}{S_{stream\_H2O}} \quad (18)$$

$$F_{streamdown\_DIN} = S_{stream\_DIN} \times \frac{F_{streamout\_H2O}}{S_{stream\_H2O}} \quad (19)$$

where all the *S* terms represent N (g N) and water stocks (m^3), and *F* terms represent flow rates of water ($m^3\ d^{-1}$) and N (g N d^{-1}) .

Temperature controls the decomposition rates of organic N in rivers (Ferreira et al., 2020). Following the algorithm of Xia et al. (2013), the rates of PON and DON decomposition in each reservoir are calculated using first-order kinetics of the corresponding N stock and a Q10 temperature dependence based on water temperature.

$$R_{fast\_PON} = S_{fast\_PON} \times K_{PON} \times Q10^{\frac{TW-T_{ref1}}{10}} \quad (20)$$

$$R_{stream\_PON} = S_{stream\_PON} \times K_{PON} \times Q10^{\frac{TW-T_{ref1}}{10}} \quad (21)$$

$$R_{fast\_DON} = S_{fast\_DON} \times K_{DON} \times Q10^{\frac{TW-T_{ref1}}{10}} \quad (22)$$

$$R_{slow\_DON} = S_{slow\_DON} \times K_{DON} \times Q10^{\frac{TW-T_{ref1}}{10}} \quad (23)$$

$$R_{stream\_DON} = S_{stream\_DON} \times K_{DON} \times Q10^{\frac{TW-T_{ref1}}{10}} \quad (24)$$

K_{PON} (0.028 d^{-1}) represents the average PON decomposition rate at 20°C in water (Islam et al., 2012); K_{DON} (0.07 d^{-1}) represents the average DON decomposition rate at the reference temperature of 20°C in water (Xia et al., 2013); *Q10* is the temperature sensitivity of PON and DON decomposition rates (= 2.0 after Liu et al., 2021; Yang et al, 2015); *TW* is the water temperature (°C); and T_{ref1} is the reference temperature for PON and DON decomposition (=20°C).

https://doi.org/10.5194/esd-2024-29
Preprint. Discussion started: 28 August 2024


Earth System Dynamics
Discussions
Open Access
EGU

The denitrification rates of DIN decrease with stream depth, because most denitrification happens in benthic sediments rather than in the water column, so high benthic area to water volume ratios result in high denitrification rates (Bernot and Dodds, 2005; Aitkenhead-Peterson et al., 2001). In addition, denitrification rates are also controlled by temperature (Jung et al., 2014; Ma et al., 2022). The denitrification is simulated by adapting the equations of Pauer et al. (2009):

$$R_{fast\_DIN} = \frac{S_{fast\_DIN}}{depth} \times K_{DIN} \times F_{T\_DIN} \quad (25)$$

$$R_{slow\_DIN} = \frac{S_{slow\_DIN}}{depth} \times K_{DIN} \times F_{T\_DIN} \quad (26)$$

$$R_{stream\_DIN} = \frac{S_{stream\_DIN}}{depth} \times K_{DIN} \times F_{T\_DIN} \quad (27)$$

$$F_{T\_DIN} = e^{\frac{-(TW-T_{ref2})^2}{T_{ref2}{}^2}} \quad (28)$$

$$depth = max\,(e^{2.56} \times Q^{0.423}, 1.0) \quad (29)$$

where K_{DIN} (0.15 d^{-1}) represents the denitrification rate in water at 25℃ (Alexander et al., 2009); F_{T_DIN} (unitless) represents the dependency of denitrification on temperature (Ma et al., 2022); T_{ref2} is the reference temperature for denitrification (=25℃); Here $\frac{1}{depth}$ (unitless) represents the factor that simulates the role of the benthic surface area to water volume ratio as a key control factor of denitrification rates. The stream *depth* is simulated according to Eq. 29 (Raymond et al., 2012). Therefore, aside from available DIN stocks, denitrification rates are spatially and temporally dependent through the effects of water residence time (controlled by topography), temperature and water depths (controlled by discharge). See Tables A1 and A2 for a summary of all variables, fluxes and processes incorporated in ORCHIDEE-NLAT.

2.2. Observational data

https://doi.org/10.5194/esd-2024-29
Preprint. Discussion started: 28 August 2024


Earth System Dynamics Discussions

Riverine water discharge from the Global Runoff Data Centre (GRDC) (Federal Institute of Hydrology, 2018) and riverine TN and NO_3^- concentrations from the Global River water Quality Archive (GRQA) (Virro et al., 2021) were used to evaluate ORCHIDEE-NLAT (Fig. 3). We retrieved GRDC water discharge data for 350 gauging stations with a catchment area greater than 50 000 km^2. From the GRQA data, only time-series with more than two observations in each month of one year were retained for model evaluation. For N concentrations, after removing duplicates in the GRQA database, we collected data of TN for 3507 sites and NO_3^- for 1841 sites. Moreover, as observations of NO_3^- at a given site are generally more frequent and cover a longer time span than for TN, we used the strong correlation between both species to estimate TN concentrations from NO_3^- if only the latter were available (yellow dots in Fig. 3). The prediction equation applied in this study (Eq. 30, Fig. S1) was obtained based on GRQA data at 148 sites with simultaneous concentrations of both TN and NO_3^- (R^2=0.78):

$$C_{TN\_obs} = 1.33 \times C_{NO3\_obs} + 0.56 \quad (30)$$

where C_{TN_obs} (g N m^{-3}) and C_{NO3_obs} (g N m^{-3}) represent the observed concentrations of TN and NO_3^-, respectively.

The TN flow rates equal to the water discharge rates multiplied by N concentrations. Therefore, for a given GRDC site, we systematically selected the nearest GRQA site with reported N concentration (McDowell et al., 2021) to calculate the flux:

$$F_{TN\_obs} = F_{W\_obs} \times C_{TN\_obs} \quad (31)$$

where F_{TN_obs} (g N d^{-1}) and F_{W_obs} (m^3 d^{-1}) represent observed rates of TN flow and water discharge, respectively.

Since TN concentrations for several large rivers (e.g., Amazon and Chinese rivers) were missing in GRQA, we complemented this dataset by

https://doi.org/10.5194/esd-2024-29
Preprint. Discussion started: 28 August 2024

collecting additional observational TN data from peer-reviewed literature (green dots in Fig. 3), resulting in the addition of 20 sites to our database, see details in Table S1.

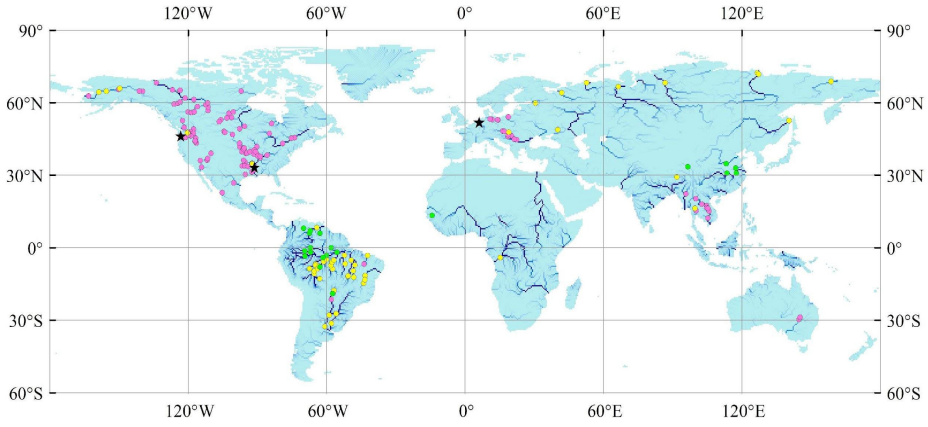

Figure 3. Location of observational sites for N concentrations. Pink dots represent sites with observations of total nitrogen (TN),116 sites; yellow dots represent sites with observations of NO_3^-, 53 sites; green dots represent sites with observations of TN from published literature, 20 sites (Table S1); and black stars represent sites with time series of water discharge and TN flow.

2.3. Simulation protocol and analysis of model results

2.3.1. Simulation protocol

ORCHIDEE-NLAT was applied to simulate the lateral transfer of PON, DON and DIN, as well as the decomposition of PON and DON, and the denitrification of DIN within the river network over the period 1901-2014. The model was run at 0.5° spatial resolution and daily temporal resolution, using the downscaled terrestrial forcings as inputs (see section 2.1.2). Running ORCHIDEE-NLAT at a daily step enables us to evaluate the model performance in simulating not only long-term trends but also the seasonality in lateral N transfers and transformations within the global river network. Model evaluation was conducted at a daily time-step by comparing the amount of simulated and observed TN lateral transfer at three sites with a long time series

https://doi.org/10.5194/esd-2024-29
Preprint. Discussion started: 28 August 2024


Earth System Dynamics
Discussions
Open Access
EGU

of observations for TN flow. We also evaluated the performance of ORCHIDEE-NLAT in simulating annual lateral TN transfer against observational data from the selected 189 sites around the world. The simulated total amounts of PON, DON and DIN from land to river and from river to ocean were further compared with previously published global N models, namely IMAGE-GNM (Vilmin et al., 2018), FrAMES-N (Frame-work for Aquatic Modeling in the Earth System) (Wollheim et al., 2008), MBM (Mass Balance Model) (Green et al., 2004), and Global NEWS2 (Mayorga et al., 2010).

Table 1 summarises the forcing and evaluation data along with their spatiotemporal resolution and references to the gridded products and point datasets.

https://doi.org/10.5194/esd-2024-29
Preprint. Discussion started: 28 August 2024

Table 1. List of forcing data needed to run ORCHIDEE-NLAT and the data used to evaluate the simulation results. S_{res} and T_{res} are the original spatial and temporal resolution of the forcing data, respectively.

.	Data	S_{res}	T_{res}	Data source
Forcing data	Runoff Drainage DOC and POC with runoff DOC and POC with drainage Soil temperature (TS)	1°	daily	ORCHIDEE-Clateral (Zhang et al., 2022)
	DIN with runoff and drainage DON leaching from manure application	2°	daily	ORCHIDEE-CNP (Sun et al., 2021)
	DIN and DON with sewage	0.5°	yearly	Beusen et al., 2014
	Flow direction Topographic index (f_{topo})	0.5°	/	Vörösmarty et al., 2000
Evaluation data	Riverine water discharge	/	daily	GRDC[a]
	Riverine TN and NO_3^- concentration	/	point measurement	GRQA[b]
	Riverine TN concentration	/	point measurement	Table S1

[a] Global Runoff Data Centre (GRDC) (Federal Institute of Hydrology, 2018); [b] Global River water Quality Archive (GRQA) (Virro et al., 2021).

2.3.2. Model evaluation metrics

To evaluate the performance of ORCHIDEE-NLAT in reproducing the spatial variations of water and N flow, the relative predictive error (RPE) and the coefficient of determination R^2 were determined. The R^2 represents how much variation in the observations can be explained by the model. The RPE quantifies the extent to which ORCHIDEE-NLAT overestimates or underestimates observations of water discharge and TN flow at grid level.

https://doi.org/10.5194/esd-2024-29
Preprint. Discussion started: 28 August 2024


Earth System Dynamics
Discussions
Open Access
EGU

$$RPE = \frac{M-O}{O} \times 100\% \quad (32)$$

where M is the mean of simulated values, O is the mean of observed values.

To assess the performance of ORCHIDEE-NLAT in reproducing time series of TN and water flows, the relative root mean square root (RRMSE) and Nash-Sutcliffe coefficient (NSE) were determined.

$$RRMSE = \frac{\sqrt{\frac{\sum_{j=1}^{n}(M_j - O_j)^2}{n}}}{\bar{O}} \times 100\% \quad (33)$$

$$NSE = 1 - \frac{\sum_{j=1}^{n}(O_j - M_j)^2}{\sum_{j=1}^{n}(O_j - \bar{O})^2} \quad (34)$$

where n represents the total number of days when observations are available at a given site; O_j and M_j represent observed and modelled values of water/TN flow on day j . NSE can take values between 1 and $-\infty$. An NSE = 1 would mean a perfect fit between observed and simulated values, NSE = 0 means that using the mean observed value as constant simulated value would lead to as much deviation between observed and predicted values as using the actual simulated values. If NSE is negative, there is more deviation between simulated and observed values than between the observed values and their mean.

2.3.3. Seasonality analysis

To explore the seasonal variability of water discharge, TN flow, TN concentration and denitrification rates during 2001-2014 at the global-scale, we constructed spatial maps of monthly anomalies following the method by Roobaert et al (2019). The FV represents the relevant flux, rate or concentration, we have that for each grid cell, the monthly anomaly of FV can be calculated as the difference between the FV value for a given month and its annual mean:

$$FVA_t^{'} = FV_t - \overline{FV} \quad (35)$$

https://doi.org/10.5194/esd-2024-29
Preprint. Discussion started: 28 August 2024


Earth System Dynamics Discussions

where FVA'_t (g N yr^{-1}) represent the anomaly of FV in month *t*, while FV_t (g N yr^{-1}) and $\overline{FV}$ (g N yr^{-1}) represent the values of FV in month *t* and for the annual mean, respectively.

The seasonality, that is the amplitude in seasonal water discharge, N flow rates, N concentrations and denitrification rates, is expressed as the root-mean-square (RMS) of the monthly FVA'.

$$season_{VA} = \sqrt{\frac{1}{12} \times \sum_1^{12} (FVA'_t)^2} \quad (36)$$

3. Results and discussion

3.1. Model evaluation

Evaluation of the water discharge results using the GRDC data indicates that for major rivers with drainage areas larger than 50 000 km^2 spread over the globe, ORCHIDEE-NLAT reproduces the magnitude and seasonal variations of water discharge well. Overall, the model simulation explains 90% of the spatial variation in the observed long-term average water discharges (Fig. 4a, Fig. S2 a). The absolute values of RPE for the simulated average water discharges are mostly smaller than 50% (Fig. S3a). At 25 sites (13% of all sites), the absolute values of RPE are larger than 100%, but the annual mean values of water discharge at each of these sites are less than 1.0×10^{11} m^3 yr^{-1}, indicating that large errors only occur at some sites draining relatively small basins (Fig. S3a). The discrepancy between model and observations at these sites may be caused by two factors: (1) a potentially substantial discrepancy between the stream routing scheme (delineation of catchment boundaries) defined by the forcing data at 0.5° resolution and the real river network; and (2) the presence of stream channel bifurcations that are poorly resolved by the model (Zhang et al., 2022). At some sites, such as the Columbia, Rhine and Mississippi Rivers,

https://doi.org/10.5194/esd-2024-29
Preprint. Discussion started: 28 August 2024


Earth System Dynamics Discussions Open Access EGU

455 ORCHIDEE-NLAT also captures the seasonal variation of the water discharges
456 well, with RRMSE ranging from 30% to 41% (Fig. 5 a1-a3).

457 Evaluation of area-averaged TN flows are overall comparable to observed
458 TN flows at the 189 sites extracted from the GRQA database and additional
459 published literature. ORCHIDEE-NLAT explains 77% of the observed spatial
460 variation of long-term TN flows across sites (Fig. 4b, Fig. S2b). The absolute
461 values of RPE of the simulated average TN flows are mostly smaller than 50%
462 (Fig. S3 b). ORCHIDEE-NLAT significantly underestimated (RPE < -100%) or
463 overestimated (RPE > 100%) the observed TN flows at 32 sites (17% of all
464 sites). Similar to water discharge, these sites are all located in relatively small
465 basins with annual water discharge less than 1.0×10^{11} m^3 yr^{-1} (Fig. S3 b). At 9
466 sites (28% of the 32 sites), the RPE of TN flow is very close to that of water
467 discharge, showing that at these sites, the water discharge (and not the N
468 concentrations) is the main reason for the discrepancies between observed and
469 modelled TN flows. The results reveal that the RPE of TN flow is relatively
470 small for large rivers, such as at sites located in the lower reaches of the
471 Columbia, Rhine and Mississippi Rivers, where RPE values are -25%, -16%
472 and 26%, respectively. ORCHIDEE-NLAT also reproduces well the seasonal
473 patterns of TN flow in these rivers, with RRMSE ranging from 30% to 64%
474 (Fig.5 b1-b3). At the Rhine river site, the NSE of TN flow is negative, reveals
475 that although the seasonal pattern of TN flow simulated by ORCHIDEE-NLAT
476 is similar to that observed, it does not capture accurate trends on the day scale
477 (Fig.5 b2).

478 The simulated DIN concentrations display broadly similar spatial patterns
479 and concentration ranges as obtained from a recent observation based machine-
480 learning (ML) based assessment (Marzadri et al., 2021). ML involves a fair
481 amount of empirical modelling, and this comparison can thus not be considered
482 as a direct model evaluation by data. Nevertheless, the agreement between both

https://doi.org/10.5194/esd-2024-29
Preprint. Discussion started: 28 August 2024

Earth System Dynamics
Discussions
Open Access
EGU

483 assessments (Fig. S4) lends further confidence in the capacity of our model to
484 realistically simulate the N cycle along the global river network.

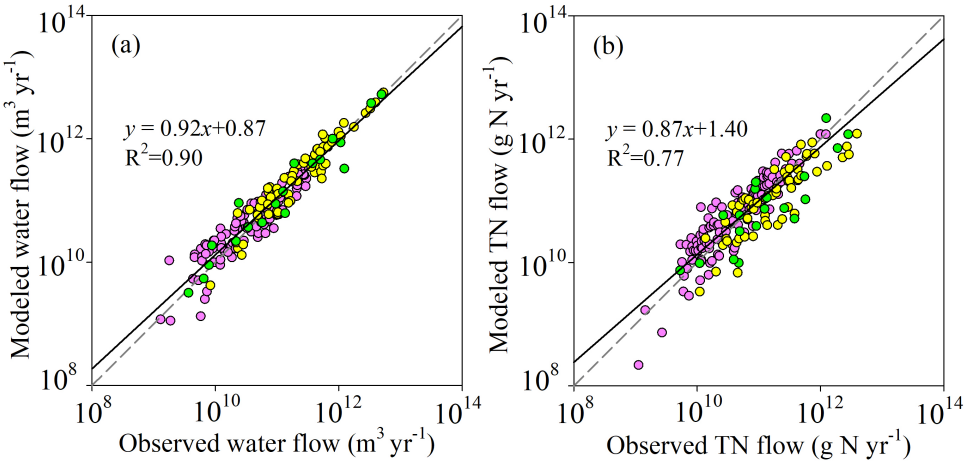

485

486 Figure 4. Evaluation of ORCHIDEE-NLAT. Global-scale comparison between
487 observed and modelled annual-mean water discharge (a) and TN flow (b). Pink
488 symbols represent sites with observations of TN from GRQA, yellow symbols
489 represent GRQA sites for which TN concentrations were estimated from
490 observations of NO_3^-, and green symbols represent sites with observations of
491 TN from published literature.

https://doi.org/10.5194/esd-2024-29
Preprint. Discussion started: 28 August 2024

Earth System Dynamics
Discussions
Open Access
EGU

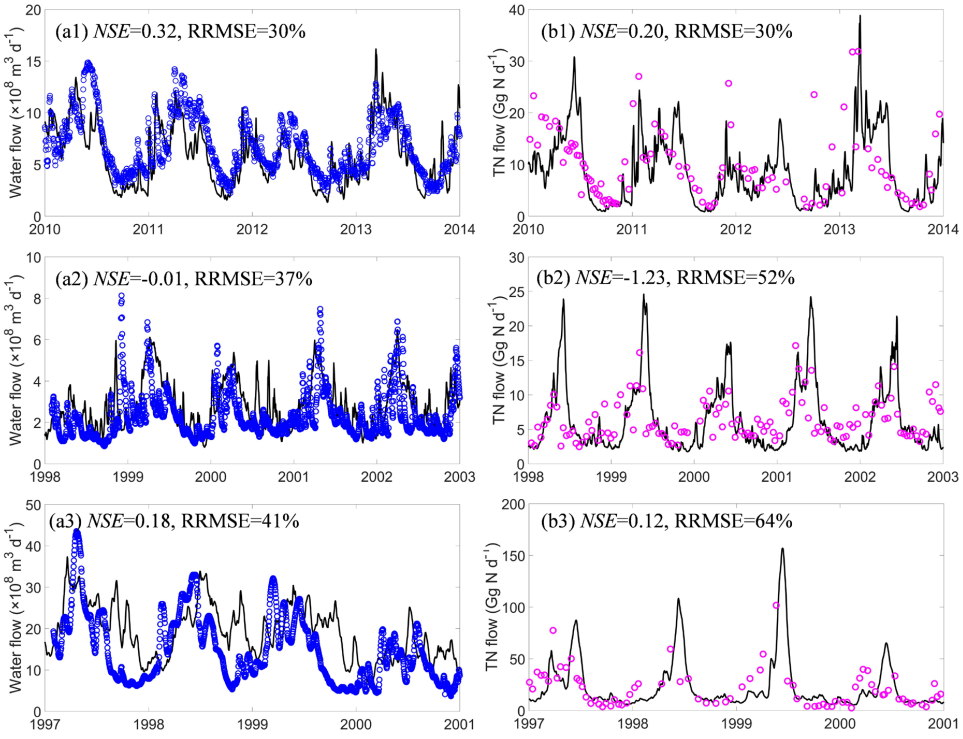

Figure 5. Time series of water discharge (a) and TN flow (b). (a1) and (b1) Columbia-river (46.18°N, 123.18°W); (a2) and (b2) Rhine-river, (51.84°N, 6.11°E); (a3) and (b3) Mississippi river (32.25°N, -91.25°W).

3.2. Temporal and spatial patterns of N flows

3.2.1. Trends in global N flows

Averaged over the 2001-2014 period, the annual TN input from soils to rivers, TN exports to oceans and denitrification in transit amount to 67.4 Tg N yr^{-1}, 40.8 Tg N yr^{-1}, and 26.6 Tg N yr^{-1}, respectively. These three N fluxes show increasing trends from 1901 to 2014. The global annual TN input to rivers increased by 82.3 %, from 36.8 Tg N yr^{-1} during 1901-1910 to 67.4 Tg N yr^{-1} during 2001-2014 (Fig. 6 a). The global annual TN exports to oceans increased by 50.4 % from 27.1 Tg N yr^{-1} to 40.8 Tg N yr^{-1}. Most of the increase in N exports to oceans is from DIN which doubled over the simulation period, from 9.6 Tg N yr^{-1} to 20.8 Tg N yr^{-1}, while DON exports show a much smaller but

https://doi.org/10.5194/esd-2024-29
Preprint. Discussion started: 28 August 2024

Earth System Dynamics
Discussions
Open Access
EGU

still substantial increase of 56.9% (Fig. 6b). In contrast, PON exports to oceans show a slightly decreasing trend. The increase in global denitrification mostly follows that of increasing DIN inputs, with a relative increase of 174.0 %, from 9.7 Tg N yr^{-1} to 26.6 Tg N yr^{-1}. The global TN input into rivers, TN exports to oceans and the denitrification in rivers all show a small peak between 1926 and 1931 due to the relatively higher surface runoff but lower belowground drainage during this period (Fig. S5). The reality of this transient peak is however questionable as it results mostly from meteorological forcing, which is uncertain for the beginning of the 20th century.

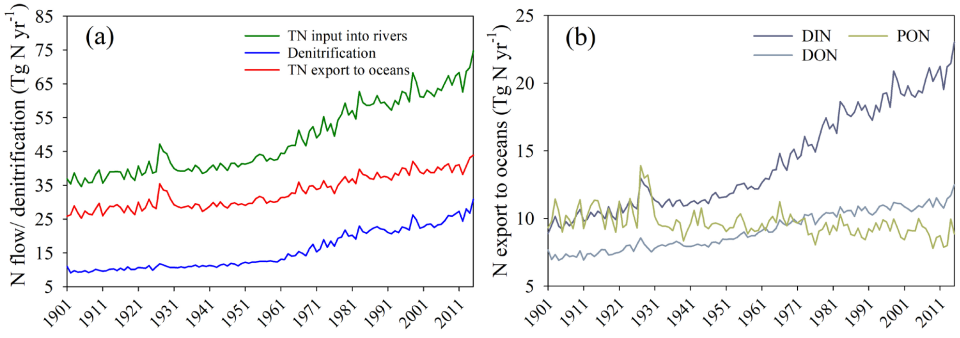

Figure 6. Trends in global N flows from 1901 to 2014: (a) TN inputs into rivers, TN exports to oceans and denitrification; (b) DIN, DON and PON exports to oceans. TN: total nitrogen; DIN: dissolved inorganic nitrogen; DON: dissolved organic nitrogen; PON: particulate organic nitrogen.

3.2.2. Spatial patterns in N flows and concentrations

Annual mean TN input into rivers during 2000-2014 shows large spatial heterogeneity, with higher values mainly located in eastern North America, South America, Western Europe, tropical Africa, South Asia, Southeast Asia and Southeast China (Fig. 7a). When compared with 1901-1910, the TN inflow into rivers increased in most areas (about 70%), with the highest increase in China exceeding 300% (Fig. 8a). Annual mean contemporary denitrification rates (2001-2014) also reveal large spatial heterogeneity (Fig. 7b) with high denitrification rates in large tropical and subtropical rivers, for example, the

https://doi.org/10.5194/esd-2024-29
Preprint. Discussion started: 28 August 2024

Amazon river, the Nile river and the Congo river. Over the entire simulation period, the grids with highest relative denitrification increases are mostly located in the subtropics (Fig. 8b).

The 2001-2014 TN export to oceans also varies substantially across regions (Fig. 7c). The riverine TN exports are relatively low for the Arctic Ocean, the western and southern coasts of Australia, and the coastal zone adjacent to desert areas in South America (e.g., the Atacama Desert and the Patagonian Desert), Africa (the Sahara Desert and the Namib Desert), and Asia (e.g., the Arabian Desert, the Thar Desert in India, the deserts of Eastern Iran, and the Syrian Desert) (Fig. 7c). On the contrary, the Amazon region in South America, African rainforest region, Western Europe, South Asia, and southeast China are prominent hot spots of riverine TN exports (Fig. 7c). Unsurprisingly, the TN export to oceans increased in most regions since the beginning of the 20th century (Fig. 8c) and in regions such as the south-eastern coastal areas of China, not only the recent TN exports to oceans are relatively high, but also the percentage increase over the 20th century exceeded 100% (Fig. 7c and Fig. 8c).

Annual mean contemporary concentration of TN at river mouths also shows large spatial heterogeneity (Fig. 7d), which differs from that of TN export to oceans (Fig. 7c). For instance, the Amazon region is one of the hotspots for TN exports, but its TN concentrations are low (<1 gN m^{-3}), because the water discharge and denitrification rates are both high (Fig. 7b, Fig. S6 a). The highest TN concentrations (>5 gN m^{-3}) are found in areas with intense human activity, for example San Francisco area, Peru, Spain, Egypt (Nile River estuary) and southeastern coastal areas of China (Bu et al., 2019; Hou et al., 2022; Yang et al., 2023).

The spatial distribution of changes in TN concentrations from 1901-1910 to 2001-2014 is also distinct from that of TN exports (Fig. 8c, d). For example, along the eastern coast of Amapá state in Brazil, and the western coast of

https://doi.org/10.5194/esd-2024-29
Preprint. Discussion started: 28 August 2024

Earth System Dynamics
Discussions
Open Access
EGU

Guinea, Sierra Leone, and Libya, TN exports to the oceans decreased by more than 20%, but TN concentrations increased by more than 10% (Fig. 8c, d). This phenomenon is due to negative trends in water discharge from the corresponding watersheds (Fig. 9, Fig. S6). In most regions, the ratio of TN concentration changes to TN flux changes is between 0 and 1, meaning that TN flux changes are the result of the joint action of changes in water and TN concentrations (TN inputs into rivers) (Fig. 9).

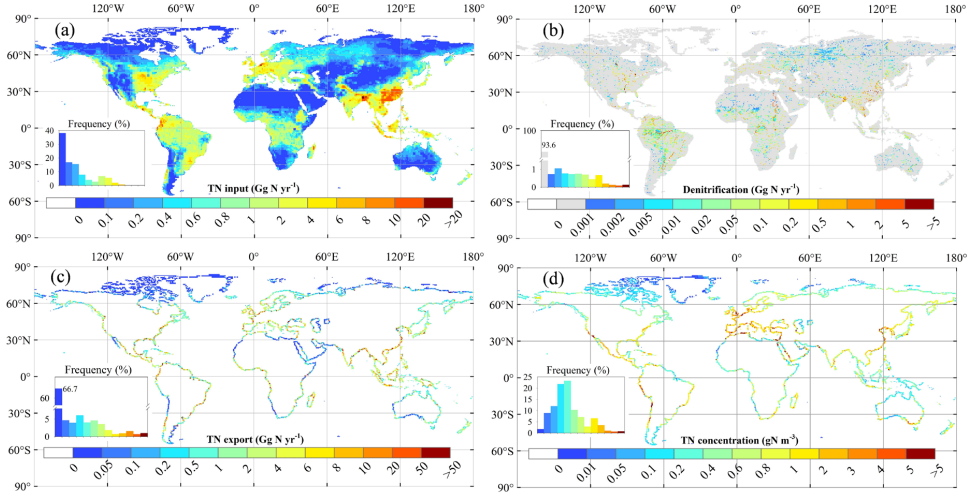

Figure 7. Spatial patterns of annual mean N fluxes and concentrations during 2001-2014: (a) TN inputs into rivers; (b) denitrification rates in rivers; (c) TN exports to oceans; (d) TN concentrations at rivers mouths. To display the spatial patterns of denitrification in rivers better, we excluded data with denitrification rates less than 0.001 GN yr^{-1} per grid.

https://doi.org/10.5194/esd-2024-29
Preprint. Discussion started: 28 August 2024

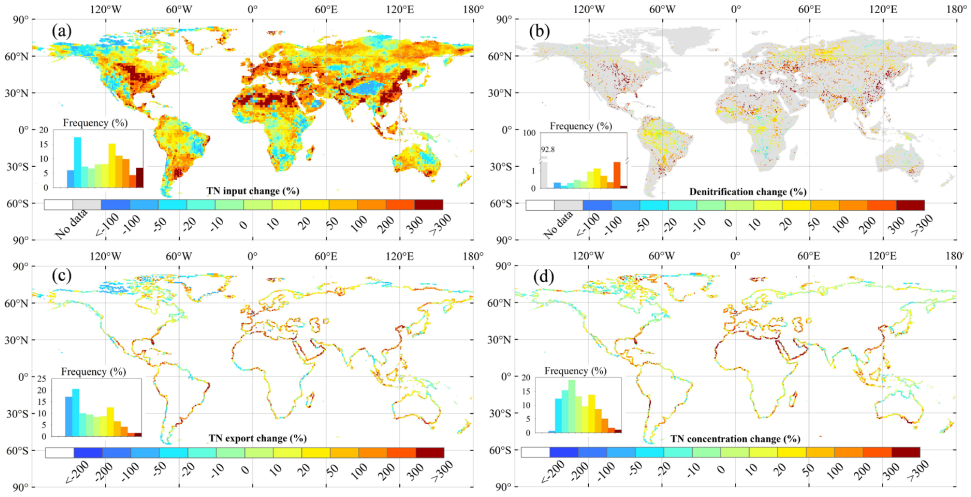

Figure 8. Spatial patterns of changes from 1901–1910 to 2001–2014 of: (a) TN inputs into rivers; (b) denitrification; (c) TN exports to oceans; (d) TN concentrations.

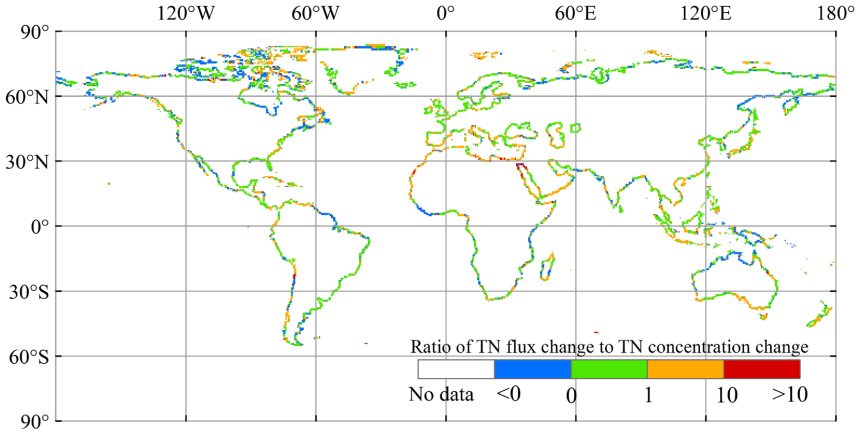

Figure 9. Ratio of TN exports changes to TN concentration changes from period 1901–1910 to 2001–2014.

3.2.3. Seasonal variability in N flows and concentrations

The seasonality of TN inputs into rivers over 2001-2014 is most pronounced in the central United States, Europe, South Asia, Southeast Asia and southeast China (Fig. 10a). The frequency distribution of the seasonal amplitude in inputs (Fig.10a) is broadly similar to that of the mean annual inputs (Fig 7a), suggesting a seasonal variability of similar magnitude than the

https://doi.org/10.5194/esd-2024-29
Preprint. Discussion started: 28 August 2024

broad, global scale spatial variability. A similar finding can also be observed for the denitrification rates, with seasonal and spatial variations of the same order of magnitude for both (Fig. 7b, 10b).

The seasonal amplitudes of TN exports to oceans over 2001-2014 shows highest values (> 10 Gg N yr^{-1}) along South Asia, and southeast China, and to a lesser extent (1-10 Gg N yr^{-1}) along the coastline of the Amazon region, the rainforest regions of Africa, Western Europe, and Mexico (Fig. 10c). Unsurprisingly, a large share of this seasonal variability is due to the river discharge (Fig. S7 a). Our results suggest that the seasonality of TN concentrations at the rivers' mouths has different spatial pattern with seasonal amplitudes of TN exports (Fig. 10c, d). This result is important because the ocean biogeochemical modelling community typically uses annual mean TN fluxes derived from Global News to force their simulations, an downscale these inputs to monthly values under the assumption that the seasonal variability of the flux is entirely due to the river discharge. Our simulations thus stresses the need for models explicitly resolving the seasonal variability of fluxes and concentrations.

We also normalized seasonalities by the mean value of nitrogen flux or concentrations. For TN inputs into reivers, denitrification and TN exports, normalized seasonal maps all show higher values in the middle and high latitudes of the Northern Hemisphere and lower values in the low latitudes and the Southern Hemisphere (Fig. S8). And it is obvious that the regional heterogeneity of normalized seasonality of TN concentration is much weaker than that of nitrogen flux (Fig. S8).

https://doi.org/10.5194/esd-2024-29
Preprint. Discussion started: 28 August 2024

Earth System Dynamics
Discussions
Open Access
EGU

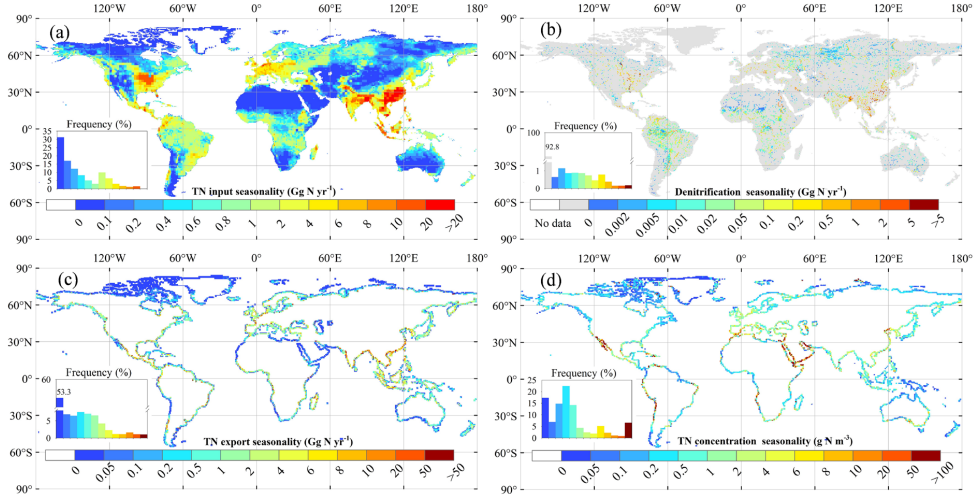

Figure 10. Spatial distribution of seasonality for TN and denitrification over 2001-2014: (a) TN inputs into rivers; (b) TN exports to oceans; (c) dnitrification removal rates; (d)TN concentrations at rivers mouths.

3.3. Comparison with other models

We compared the trends of global N input to rivers simulated by ORCHIDEE-NLAT and the recently published IMAGE-GNM (Vilmin et al., 2018). Overall, both models capture a similar increasing trend of global DIN delivery from land to rivers from 1901 till 2001 (Fig. 11a). During 1961-2000, the global-scale interannual variability of DIN simulated by ORCHIDEE-NLAT is comparatively stronger than that simulated by IMAGE-GNM (Fig. 11a). To some extent, this could be due to the different temporal resolution of the two models (daily for ORCHIDEE-NLAT, yearly for IMAGE-GNM) and their associated climate forcings. That is, ORCHIDEE-NLAT calculates annual means from daily fluxes, while IMAGE-GNM does not resolve the intra-annual variability. The results however markedly differ regarding organic N (ON=PON+DON) with IMAGE-GNM simulating a significant increase from 24.9 Tg N yr^{-1} during 1901-1910 to 37.9 Tg N yr^{-1} in during 1990-2000, while the ON inflow simulated by ORCHIDEE-NLAT shows a weaker increasing trend over the same period (26.5 Tg N yr^{-1} during 1901-1910 to 32.4 Tg N yr^{-1}

https://doi.org/10.5194/esd-2024-29
Preprint. Discussion started: 28 August 2024

628 during 1990-2000). The weaker trend in our model can primarily be explained
629 by the increasing DON inflow being offset by a decreasing PON inflow (Fig.
630 11c). The fundamental reason for the discrepancy among the two models stems
631 from their distinct structures and algorithms. In ORCHIDEE-NLAT, the ON
632 flows into rivers are calculated separately for the dissolved and particulate
633 compounds using a process-based representation of the soil C stock dynamics
634 and C:N ratios, as well as the rates of runoff and drainage. The approach is
635 different in IMAGE-GNM which calculates the bulk ON flows (DON+PON)
636 based on empirical formulas (Vilmin et al., 2018). Specifically, it calculates the
637 ON delivery from land to rivers with drainage based on the TN delivery rate,
638 assuming that 50% of this flux is in the form of ON. For ON flows into rivers
639 with runoff, IMAGE-GNM distinguishes two runoff mobilisation pathways, i.e.
640 losses from recent nutrient applications in forms of fertiliser and manure, and a
641 memory effect related to long-term historical changes in soil nutrient
642 inventories. These two pathways are simulated based on empirical formulas
643 (Vilmin et al., 2018). In ORCHIDEE-NLAT, we used default C:N ratios (from
644 ORCHIDEE-Clateral) in different SOM pools to calculate the PON flow out of
645 soils, and a constant C:N ratio (averaged values from references) to simulate
646 DON flow out of soils. The assumption of constant C:N ratio for dissolved
647 matter in soil could to some extent contribute to the weaker trend in ON
648 delivery to rivers simulated by ORCHIDEE-NLAT, since some studies have
649 revealed that DOC:DON ratios vary with time and land cover (Li et al., 2019;
650 Yates et al., 2019).

https://doi.org/10.5194/esd-2024-29
Preprint. Discussion started: 28 August 2024

Earth System Dynamics
Discussions
Open Access
EGU

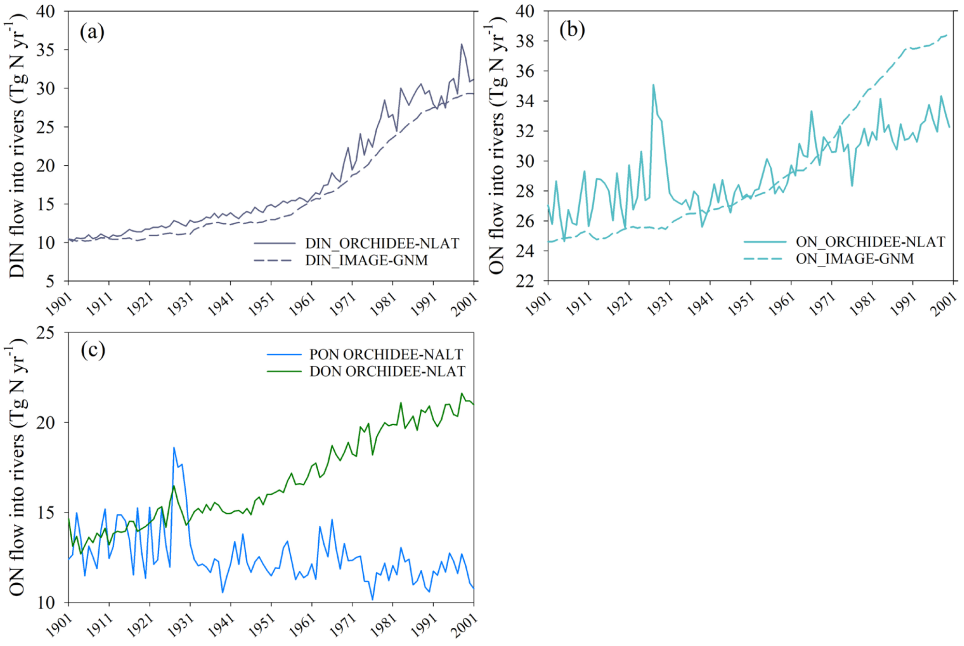

Figure 11. Global terrestrial N flows into rivers from 1901 to 2001 simulated by ORCHIDEE-NLAT and IMAGE-GNM (Vilmin et al., 2018): (a) DIN; (b) ON (DON+PON); (c) DON and PON simulated by ORCHIDEE-NLAT.

The simulated lateral N flows from land to rivers and N exports to oceans in this study are now compared with those simulated by other models for different time horizons, noting that each model covers different time periods (Fig. 12a). Focusing first on the global N flows from land to rivers, we find that for different time horizons, the simulated N input by ORCHIDEE-NLAT is very close with those estimated by IMAGE-GNM (Vilmin et al., 2018) and FrAMES-N (Wollheim et al., 2008) with differences between ORCHIDEE-NLAT and other models for the different time horizons never exceeding 7%. Although the fraction of DIN in TN over 1901-1910 simulated by ORCHIDEE-NLAT (27%) is slightly lower than that of IMAGE-GNM (29%), the DIN fractions simulated by these two models both show obvious increasing trends with time, ORCHIDEE-NLAT and IMAGE-GNM reporting DIN fractions for the 1991-2000 period reaching 48% and 43%, respectively. A comprehensive

https://doi.org/10.5194/esd-2024-29
Preprint. Discussion started: 28 August 2024

668 cross-biome assessment of N composition in rivers also found that the dissolved
669 N pool shifts from highly heterogeneous to primarily inorganic N in response to
670 human disturbances (Wymore et al., 2021). Changes in the composition of TN
671 inputs from land to rivers is primarily caused by the excess inorganic N release
672 from agricultural (due to the utilisation of fertilisers) and urban (due to the
673 release of sewage) areas.

674 The global N export from rivers to oceans simulated by ORCHIDEE-
675 NLAT is also comparable to the estimates from other models. During 1901-
676 1910, the global riverine N export to oceans is 29.0 Tg N yr^{-1}, within the range
677 of values simulated by IMAGE-GNM (19.0 Tg N yr-1, Vilmin et al., 2018) and
678 DLEM (29.4 Tg N yr^{-1}, Tian, pers. com.) (Fig. 12b). For the most recent period
679 (2000s), the simulated riverine N export to oceans is converging, with
680 differences smaller than 10 % compared to other models such as GlobaNEWS2
681 (Mayorga et al., 2010), IMAGE-GNM, and DLEM (Fig. 12b). Although the
682 global riverine TN export to oceans simulated by ORCHIDEE-NLAT is close to
683 that simulated by GlobalNEWS2 (1970-2010), the TN export reported here
684 contains a slightly larger fraction of DIN and a slightly lower fraction of PON
685 compared to GlobalNEWS2 (Fig. 12b).

686 The TN export to oceans simulated by ORCHIDEE-NLAT and
687 GlobalNEWS2 are also comparable at continental scale (Fig. 13a), with largest
688 TN exports from Asia, and lowest exports from Australia. However, the
689 simulated proportions of N species in the overall TN export show distinct
690 behaviour between these two models. For example, compared to
691 GlobalNEWS2, the DIN proportion in TN exports simulated by ORCHIDEE-
692 NLAT is larger in Asia, Africa and South America but smaller in Europe (Fig.
693 13a).

694 The magnitude of TN exports simulated by ORCHIDEE-NLAT and
695 GlobalNEWS2 continue to diverge at basin scale (Fig. 13b). In 8 of the top 20

https://doi.org/10.5194/esd-2024-29
Preprint. Discussion started: 28 August 2024

basins by area, the difference between the two models is less than 50%, such as the Congo, the Mississippi, the Ob, the Parana, the Yenisei, the Changjiang, the Mackenzie and the Nelson. Larger discrepancies can even be observed for several large river systems. For instance, in the Amazon basin, the TN export simulated by GlobaNEWS2 is about 2.5 times larger than that simulated by ORCHIDEE-NLAT. Evaluation of ORCHIDEE-NLAT simulation results against measurements of TN flow rates in the Amazon River indicates that ORCHIDEE-NLAT underestimates the TN flow in this basin (Fig. S2). At the Manacapuru and the Óbidos, two observation sites on the main channel of the Amazon River, the observed TN flow is 1.90 Tg N yr^{-1} and 2.82 Tg N yr^{-1}, but the simulated values are 0.92 Tg N yr^{-1} and 1.57 Tg N yr^{-1}, respectively. To evaluate whether the underestimation is caused by less TN inflow into rivers, we set the river transformation processes to zero, and found that the TN flow is 1.56 Tg N yr^{-1} at the Manacapuru site and 2.35 Tg N yr^{-1} at the Óbidos site. Therefore, even with no N removal ORCHIDEE-NLAT still underestimates the observed TN flows at these two sites , a finding suggesting that N delivery from terrestrial ecosystems is too low in the Amazon basin by ORCHIDEE-NLAT. In the Nile basin, the TN export simulated by ORCHIDEE-NLAT is thirty times larger than that simulated by GlobalNEWS2. The observed annual exports of DIN and DON amount to 0.079 Tg N yr^{-1} and 0.038 Tg N yr^{-1}, respectively (Badr, 2016). These observed values are of the same magnitude with those of ORCHIDEE-NLAT reaching 0.113 Tg N yr^{-1} for DIN and 0.048Tg N yr^{-1} for DON. suggesting that our model better captures the observed N export for this specific basin than GlobalNEWS2.

It should be noted that the GlobalNEWS2 and IMAGE-GNM both have IMAGE part to simulated N inputs into inland water, but they were developed based on different hydrological models and use different methods to calculate N transport and retention. The hydrological model used in GlobalNEWS2 is Water

https://doi.org/10.5194/esd-2024-29
Preprint. Discussion started: 28 August 2024


Earth System Dynamics
Discussions
Open Access
EGU

724 Balance Model (WBM_{plus}) (Fekete et al., 2010) , and NEWS models were used
725 to calculate nutrient retention in streams and reservoirs (Seitzinger et al., 2005,
726 2010; Mayorga et al., 2010). The hydrological model ued in IMAGE-GNM is
727 Global Water Balance (PCR-GLOBWB) (Van Beeket al., 2011), and IMAGE-
728 GNM uses the nutrient spiraling approach (Newbold et al., 1981) to describe in-
729 stream retention of both N and P with a yearly time step (following Wollheim et
730 al., 2008).

731 In summary, the global total N input to rivers and N export to oceans
732 simulated by the different models are comparable, but the spatial distribution of
733 N export to oceans at finer spatial scales shows increasing discrepancies, as
734 does the chemical speciation. This is mainly due to differences in model
735 structures, spatial and temporal resolutions and forcing data. Albeit our model
736 has been evaluated against the largest dataset of river discharge and N
737 concentrations from the recently assembled global GRQA database, the
738 significant cross-model discrepancies that emerge as the analysis is refined to
739 regional patterns and single species urgently calls for ensemble-means
740 assessments, similar to what has recently been performed for C exports to the
741 ocean (Liu et al., 2024).

https://doi.org/10.5194/esd-2024-29
Preprint. Discussion started: 28 August 2024

Earth System Dynamics
Discussions
Open Access
EGU

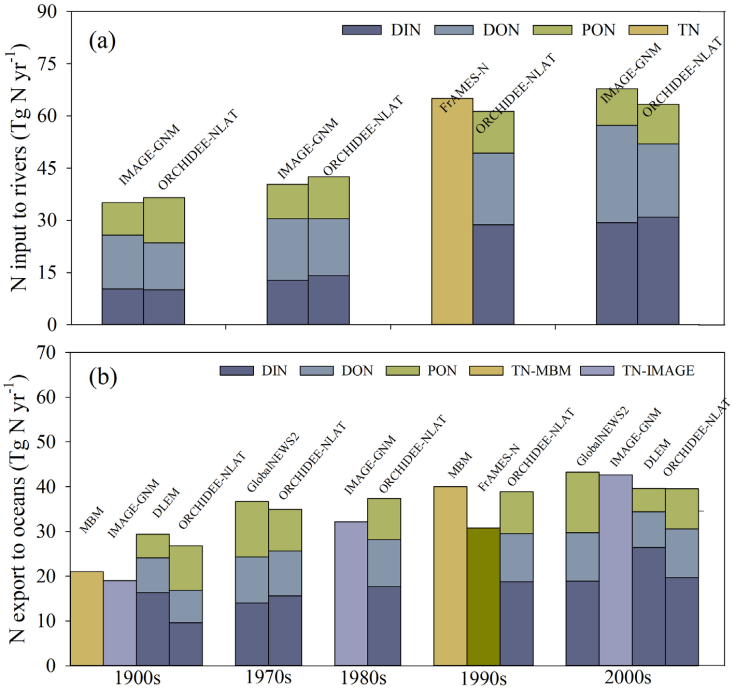

Figure 12. Comparison of global TN fluxes estimated by different models: (a) global TN inputs to rivers; (b) global TN exports to oceans. IMAGE-GNM: Integrated Model to Assess the Global Environment-Global Nutrient Model (Vilmin et al., 2018); FrAMES-N: Frame-work for Aquatic Modeling in the Earth System (Wollheim et al., 2008); MBM: Mass Balance Model (Green et al., 2004); Global NEWS2: Global Nutrient Export from Watersheds 2 (Mayorga et al., 2010); DLEM, Dynamic Land Ecosystem Model, unpublished (Tian, pers. com.).

https://doi.org/10.5194/esd-2024-29
Preprint. Discussion started: 28 August 2024

Earth System Dynamics
Discussions
Open Access
EGU

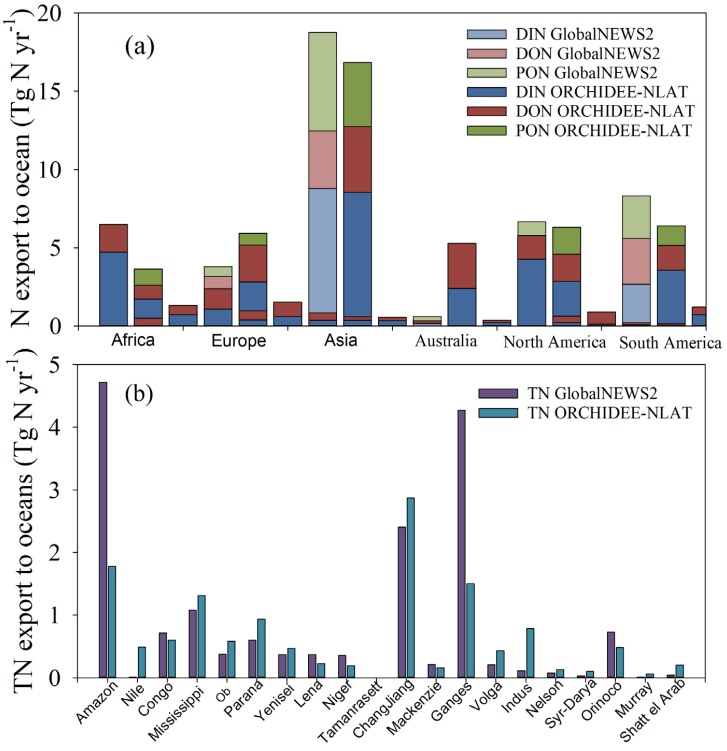

Figure 13. Comparison of TN export to oceans simulated by ORCHIDEE-NLAT and GlobalNEWS2: (a) at continental scale over 2001-2010 (Mayorga et al., 2010); (b) at basin scale over 2001-2010.

3.4. Some limitations to keep in mind

ORCHIDEE-NLAT currently relies on a simplified representation of the N processes in benthic sediments and water, without explicit simulation of the hyporheic exchange between sediments and water, instead estimating the importance of these processes via a scaling factor based on water depth. This scaling itself relies on a coarse estimate of the stream channel geometry based on empirical formulas (Raymond et al., 2012). Global-scale databases on the geomorphic properties of global river channels including river depth and width however exist (Andreadis et al., 2013) and could be used in the future to further refine the representation of N processes in river channels, including the hyporheic exchange between sediments and water. The use of a constant C:N

https://doi.org/10.5194/esd-2024-29
Preprint. Discussion started: 28 August 2024

766 ratio to simulate DON fluxes from soils to rivers is another limitation of
767 ORCHIDEE-NLAT, since it has been shown to vary over time and land cover
768 type (Li et al., 2019; Yates et al., 2019). In addition, few studies have focused
769 on the influence of PON deposition and resuspension on lateral N transfer in
770 rivers because of the difficulty to represent these processes on the global-scale.

771 The role of autotrophic production is another process currently omitted
772 Autotrophs (aquatic macrophytes, algae, cyanobacteria, bryophytes, some
773 protists, and bacteria) in freshwater consume N through photosynthesis (King et
774 al., 2014) and may play a significant role in river N cycling. For instance, a
775 long-term study has shown that as pollution from industrial and wastewater
776 emissions decreased, in-situ gross primary production increased, prompting a
777 shift from heterotrophic-dominated (i.e. controlled mainly by nitrification and
778 denitrification) towards autotrophic-dominated N retention regime in rivers
779 (Wachholz et al., 2024). In the future, the role of autotrophic production on N
780 retention should thus be considered, although the large dominance of the
781 heterotrophic metabolism on a global scale suggests that in-situ aquatic
782 production is likely a second-order control (Battin et al., 2023).

783 In the present version of ORCHIDEE-NLAT, river-floodplain dynamics
784 and channel erosion are currently not represented, because of the incomplete
785 understanding of the effects of these processes on lateral N transfer, the lack of
786 reliable parameters from field studies to calculate the effects of these processes
787 at global scale. Floodplain inundation does not only carry N into river, but also
788 has a significant impact on N retention efficiency in rivers (Martí et al., 1997;
789 Hanrahan et al., 2018), and N cycling (e.g., nitrification and denitrification) in
790 flooded soils (Sánchez-Rodríguez et al., 2019; Hu et al., 2020). For instance, in
791 the Jiulong River watershed, southeast China, flood events exported 47% and
792 42 % of the annual land-derived ammonium (NH_4^+) and NO_3^-, respectively,
793 although they only occurred 24% of the time (Gao et al., 2018).

https://doi.org/10.5194/esd-2024-29
Preprint. Discussion started: 28 August 2024

794 ORCHIDEE-NLAT includes the major sources of riverine N with runoff
795 and drainage in natural, agricultural and urban ecosystems (Fig. 1). Yet, several
796 sources are still missing, for example atmospheric N deposition directly onto
797 rivers and N release from aquaculture (Filoso et al., 2003; Bouwman et al.,
798 2013; Beusen et al., 2016; Gao et al., 2020), suggesting that the N exports to
799 oceans simulated by ORCHIDEE-NLAT might be conservative. On the other
800 hand, N retention and recycling in lakes and artificial reservoirs are currently
801 missing, which have the potential to decrease lateral N flows because they offer
802 ideal conditions for N burial in sediment or permanent loss via denitrification
803 (Saunders & Kalff, 2001; Harrison et al., 2009; Akbarzadeh et al., 2019).

804 Forcing data used by the ORCHIDEE-NLAT (Table 1) introduces
805 additional uncertainties in the simulation results. The routing scheme of water
806 and N is driven by a map of streamflow direction at 0.5◦ spatial resolution
807 (Vörösmarty et al., 2000, https://doi.org/10.1016/S0022-1694(00)00282-1).
808 There are obvious discrepancies between this routing scheme and the real river
809 network (Zhang et al., 2022). Deviation of flow direction induces uncertainties
810 in the simulated riverine water discharge and N flow because the flow direction
811 directly determines the area of each catchment and the routing of the river.

812 Finally, although ORCHIDEE-NLAT reproduces the magnitude and
813 seasonal variations of water and N transfer from land to rivers and oceans well
814 (Fig. 4, 5), spatial and temporal biases in observational data also affect the
815 evaluation of model results. Most observations of riverine N are distributed in
816 North America, South America and Europe. and there is thus a crucial need to
817 collect more measurements in other regions of the world, especially in Africa.
818 In addition, despite the strong correlation between TN and NO_3^- concentrations,
819 the application of the resulting empirical equation (Eq. 30) also adds
820 uncertainties in the observational dataset (Pisani et al., 2017; Niu et al., 2022).

https://doi.org/10.5194/esd-2024-29
Preprint. Discussion started: 28 August 2024

4. Conclusions

We developed a global N lateral transfer model from land to oceans through the river network, including the decomposition of DON and PON and denitrification of DIN during fluvial transport. Evaluations using observation data from GRDC and GRQA indicate that ORCHIDEE-NLAT reproduce observed rates and seasonal variations of water discharge and N flow well. The global simulations of ORCHIDEE-NLAT shows that global TN inputs into rivers, TN exports to oceans and denitrification rates in rivers increased significantly over the last century. In particular, the TN export to oceans increased from 27.1 Tg N yr^{-1} during 1901-1910 to 40.8 Tg N yr^{-1} during 2001-2014, with DIN contributing 80% to the TN increase. Our results reveal significant spatial heterogeneity in the global distribution of N inputs, transformation and exports to oceans, with East Asia and Southeast Asia as hotspots of N lateral transfers and their increase. The seasonal amplitude of TN exports are of similar magnitude than the large-scale spatial heterogeneity in TN fluxes. Although the global and continental-scale TN export to oceans simulated by ORCHIDEE-NLAT is similar to that of another widely used model (GlobalNEWS2), their spatial distribution at the basin scale reveals significant discrepancies. One key strength of ORCHIDEE-NLAT is its ability to resolve N processes at the daily timescale, using a framework fully compatible with land surface model outputs, hence allowing to account for the effects of climate change, atmospheric composition changes, land-use change, and agricultural practices (e.g., manure and fertiliser use) in a fully consistent way.

ORCHIDEE-NLAT has however its own limitations and we plan to further enhance its capabilities with additional processes (e.g. autotrophy, variable C:N ratios, erosion-deposition on river bed), additional sources (e.g. aquaculture, direct N deposition) and interconnections with other (semi)-aquatic and benthic systems (hyporheic zone, lakes, reservoirs, floodplains). We will also continue

https://doi.org/10.5194/esd-2024-29
Preprint. Discussion started: 28 August 2024


Earth System Dynamics Discussions Open Access EGU

to collect more observation data to further calibrate and evaluate ORCHIDEE-NLAT. Last but not least, ORCHIDEE-NLAT is currently being dynamically embedded into ORCHIDEE-3 (Vuichard et al., 2019), the land surface scheme embedded in the IPSL Earth System Model opening new avenues towards fully coupled simulations of the land-ocean-atmosphere N cycle. The current offline version of our model could also be easily coupled to other LSMs representing N cycling in terrestrial ecosystems.

https://doi.org/10.5194/esd-2024-29
Preprint. Discussion started: 28 August 2024

Earth System Dynamics Discussions
Open Access
EGU

857 **Appendices**

858 Table A1. Abbreviation used in the text.

Abbreviation	Meaning	unit
F_{DR_DIN}	leaching rates of DIN with drainage	g N d^{-1}
F_{DR_DON}	leaching rates of DON with drainage	g N d^{-1}
F_{RO_DIN}	leaching rates of DIN with runoff	g N d^{-1}
F_{RO_DON}	leaching rates of DON with runoff	g N d^{-1}
F_{RO_PON}	erosion rates of PON with runoff	g N d^{-1}
F_{sewage_DIN}	DIN inflow rates from sewage	g N d^{-1}
F_{sewage_DON}	DON inflow rates from sewage	g N d^{-1}
$F_{fastout\_H2O}$	outflow rates of water from fast reservoirs to stream reservoirs	m^3 d^{-1}
$F_{fastout\_DIN}$	outflow rates of DIN from fast reservoirs to stream reservoirs	g N d^{-1}
$F_{fastout\_DON}$	outflow rates of DON from fast reservoirs to stream reservoirs	g N d^{-1}
$F_{fastout\_PON}$	outflow rates of PON from fast reservoirs to stream reservoirs	g N d^{-1}
$F_{slowout\_H2O}$	outflow rates of water from slow reservoirs to stream reservoirs	m^3 d^{-1}
$F_{slowout\_DIN}$	outflow rates of DIN from slow reservoirs to stream reservoirs	g N d^{-1}
$F_{slowout\_DON}$	outflow rates of DON from slow reservoirs to stream reservoirs	g N d^{-1}
$F_{streamout\_H2O}$	outflow rates of H_2O to downstream reservoirs	m^3 d^{-1}
$F_{streamout\_DIN}$	outflow rates of DIN to downstream reservoirs	g N d^{-1}
$F_{streamout\_DON}$	outflow rates of DON to downstream reservoirs	g N d^{-1}
$F_{streamout\_PON}$	outflow rates of PON to downstream reservoirs	g N d^{-1}
R_{fast_DIN}	denitrification rates in fast reservoirs	g N d^{-1}
R_{fast_DON}	decomposition rates of DON in fast reservoirs	g N d^{-1}
R_{fast_PON}	decomposition rates of PON in fast reservoirs	g N d^{-1}
R_{slow_DIN}	denitrification rates in slow reservoirs	g N d^{-1}
R_{slow_DON}	decomposition rates of DON in slow reservoirs	g N d^{-1}
R_{stream_DIN}	denitrification rates in stream reservoirs	g N d^{-1}
R_{stream_DON}	decomposition rates of DON in stream reservoirs	g N d^{-1}
R_{stream_PON}	decomposition rates of PON in stream reservoirs	g N d^{-1}
S_{fast_H2O}	water stock in fast reservoir	m^3
S_{fast_DIN}	DIN stock in fast reservoir	g N
S_{fast_DON}	DON stock in fast reservoir	g N
S_{fast_PON}	PON stock in fast reservoir	g N
S_{slow_H2O}	water stock in slow reservoir	m^3
S_{slow_DIN}	DIN stock in slow reservoir	g N
S_{slow_DON}	DON stock in slow reservoir	g N
S_{stream_H2O}	water stock in stream reservoir	m^3
S_{stream_DIN}	DIN stock in stream reservoir	g N
S_{stream_DON}	DON stock in stream reservoir	g N
S_{stream_PON}	PON stock in stream reservoir	g N
TW	water temperature	℃
F_{T_DIN}	dependency of denitrification on temperature	unitless

https://doi.org/10.5194/esd-2024-29
Preprint. Discussion started: 28 August 2024

Earth System Dynamics
Discussions
Open Access
EGU

depth	depth of rivers	m
Q	water discharge	$m^3\ yr^{-1}$

Table A2. Values of the key parameters used in ORCHIDEE-NLAT to simulate the lateral transfer of N.

Parameter	Value	Description	Source
τ_{fast}	3.0 days	A factor which translates the topographic index into the water residence time of the "fast" reservoir (Eq. 1)	Ngo-Duc et al., 2006
τ_{slow}	25.0 days	A factor which translates the topographic index into the water residence time of the "slow" reservoir (Eq. 2)	Ngo-Duc et al., 2006
τ_{stream}	0.24 days	A factor which translates the topographic index into the water residence time of the "stream" reservoir (Eq. 3)	Ngo-Duc et al., 2006
K_{PON}	0.028 d^{-1}	the average PON decomposition rate at 20°C in water (Eqs. 20-21)	Islam et al., 2012
K_{DON}	0.07 d^{-1}	the average DON decomposition rate at 20°C in water (Eqs. 22-24)	Xia et al., 2013
K_{DIN}	0.15 d^{-1}	the average denitrification rate in water at 25°C (Eqs. 25-27)	Alexander et al., 2000
Q_{10}	2.0	the temperature sensitivity of PON and DON decomposition rates (Eqs. 20-24)	Liu et al., 2021 Zang et al., 2020
T_{ref1}	20 °C	the reference temperature for PON and DON decomposition (Eqs. 20-24)	
T_{ref2}	25 °C	the reference temperature for denitrification (Eq. 28)	Ma et al., 2022

https://doi.org/10.5194/esd-2024-29
Preprint. Discussion started: 28 August 2024

862 **Code and data availability.** The source code of the ORCHIDEE-NLAT model
863 is available online (http://doi.org/10.5281/zenodo.13309551). All forcing and
864 validation data used in this study are publicly available online. The specific
865 sources for these data can be found in Table 1.
866
867 **Author contributions.** MM, HZ, RL, PR and PC designed the study. MM and
868 HZ conducted the model development and simulation experiments. PR, RL and
869 PC provided critical contributions to the model development and the design of
870 simulation experiments. MM conducted the model calibration, validation, and
871 data analysis. HZ, PR, RL and PC provided support on collecting forcing and
872 validation data. MM wrote the paper. All authors contributed to interpretation
873 and discussion of results and improved the paper.

874 **Competing interests.** The contact author has declared that none of the authors
875 has any competing interests.

876

877 **Acknowledgements.** MM and PR acknowledge funding from the European
878 Union's Horizon 2020 research and innovation program under grant agreement
879 no. 101003536 (ESM2025 – Earth System Models for the Future). P.R. received
880 financial support from BELSPO through the project ReCAP (which is part of
881 the Belgian research programme FedTwin). HZ acknowledges the Fundamental
882 and Applied Basic Research Fund of Guangdong Province, China (No.
883 2024A1515010929) and the Fundamental Research Funds for the Central
884 Universities, Sun Yat-sen University (No. 31610004). PC and RL acknowledge
885 support from the CLAND convergence institute funded by the National
886 Research Agency of France 'ANR' 16-CONV-0003. PC also acknowledges
887 support of the CALIPSO project funded through the generosity of Eric and
888 Wendy Schmidt by recommendation of the Schmidt Futures program. RL and

https://doi.org/10.5194/esd-2024-29
Preprint. Discussion started: 28 August 2024

889 PR further acknowledge funding under the ‘France 2030’ programme with the
890 reference ANR-22-PEXF-0009 (PEPR ‘FairCarboN’—project ‘DEEP-C’). We
891 thank Hanqin Tian’s team for providing the simulated data from DLEM.

892

https://doi.org/10.5194/esd-2024-29
Preprint. Discussion started: 28 August 2024

Earth System Dynamics Discussions

References

Aitkenhead-Peterson, J. A., J. E. Alexander, and T. A. Clair.: Dissolved Organic Carbon and Dissolved Organic Nitrogen Export from Forested Watersheds in Nova Scotia: Identifying Controlling Factors, Global Biogeochemical Cycles, 19, GB4016, https://doi.org/10.1029/2004GB002438, 2018.

Akbarzadeh, Zahra, Taylor Maavara, Stephanie Slowinski, and Philippe Van Cappellen.:Effects of Damming on River Nitrogen Fluxes: A Global Analysis, Global Biogeochemical Cycles, 33,1339–57, https://doi.org/10.1029/2019GB006222, 2019.

Alexander, Richard B., John Karl Böhlke, Elizabeth W. Boyer, Mark B. David, Judson W. Harvey, Patrick J. Mulholland, Sybil P. Seitzinger, Craig R. Tobias, Christina Tonitto, and Wilfred M. Wollheim.: Dynamic Modeling of Nitrogen Losses in River Networks Unravels the Coupled Effects of Hydrological and Biogeochemical Processes, Biogeochemistry, 93, 91–116. https://doi.org/10.1007/s10533-008-9274-8, 2019.

Andreadis, Konstantinos M., Guy J.-P. Schumann, and Tamlin Pavelsky.: A Simple Global River Bankfull Width and Depth Database, Water Resources Research, 49, 7164–68, https://doi.org/10.1002/wrcr.20440, 2013.

Arnold, J. G., R. Srinivasan, R. S. Muttiah, and J. R. Williams.: LARGE AREA HYDROLOGIC MODELING AND ASSESSMENT PART I: MODEL DEVELOPMENT, JAWRA Journal of the American Water Resources Association, 34, 73–89, https://doi.org/10.1111/j.1752-1688.1998.tb05961.x, 1998.

Badr, El-Sayed A.: Spatio-Temporal Variability of Dissolved Organic Nitrogen (DON), Carbon (DOC), and Nutrients in the Nile River, Egypt, Environmental Monitoring and Assessment, 188, 580, https://doi.org/10.1007/s10661-016-5588-5, 2016.

Battin, Tom J., Ronny Lauerwald, Emily S. Bernhardt, Enrico Bertuzzo, Lluís Gómez Gener, Robert O. Hall, Erin R. Hotchkiss, et al.: River Ecosystem Metabolism and Carbon Biogeochemistry in a Changing World, Nature, 613, 449–59. https://doi.org/10.1038/s41586-022-05500-8, 2023.

Bernot, Melody J., and Walter K. Dodds.: Nitrogen Retention, Removal, and Saturation in Lotic Ecosystems, Ecosystems, 8, 442–53, https://doi.org/10.1007/s10021-003-0143-y, 2005.

Beusen, A. H. W., L. P. H. Van Beek, A. F. Bouwman, J. M. Mogollón, and J. J. Middelburg.: Coupling Global Models for Hydrology and Nutrient Loading to Simulate Nitrogen and Phosphorus Retention in Surface

https://doi.org/10.5194/esd-2024-29
Preprint. Discussion started: 28 August 2024

Water – Description of IMAGE–GNM and Analysis of Performance, Geoscientific Model Development, 8, 4045–67, https://doi.org/10.5194/gmd-8-4045-2015, 2015.

Beusen, A. H. W., A. F. Bouwman, L. P. H. Van Beek, J. M. Mogollón, and J. J. Middelburg.: Global Riverine N and P Transport to Ocean Increased during \hack\newlinethe 20th Century despite Increased Retention \hack\newlinealong the Aquatic Continuum, Biogeosciences, 13, 2441–51, https://doi.org/10.5194/bg-13-2441-2016, 2016.

Beusen, Dr. A.H.W. (PBL Netherlands Environmental Assessment Agency / Utrecht University); Planbureau voor de Leefomgeving - PBL: Global riverine nitrogen (N) and phosphorus (P) input, retention and export during the 20th century. DANS. https://doi.org/10.17026/dans-zgs-9k9m, 2016.

Beusen, A.H.W., J.C. Doelman, L.P.H. Van Beek, P.J.T.M. Van Puijenbroek, J.M. Mogollón, H.J.M. Van Grinsven, E. Stehfest, D.P. Van Vuuren, and A.F. Bouwman.: Exploring River Nitrogen and Phosphorus Loading and Export to Global Coastal Waters in the Shared Socio-Economic Pathways, Global Environmental Change, 72, https://doi.org/10.1016/j.gloenvcha.2021.102426, 2022.

Bicknell, B. R., J. J. Burkey, and R. A. Dusenbury.: Modeling Water Quality in Urban Northwest Watersheds. In Managing Watersheds for Human and Natural Impacts, 1–12, https://doi.org/10.1061/40763(178)93, 2005.

Billen, Gilles, Josette Garnier, and Luis Lassaletta.: The Nitrogen Cascade from Agricultural Soils to the Sea: Modelling Nitrogen Transfers at Regional Watershed and Global Scales, Philosophical Transactions of the Royal Society B: Biological Sciences, 368, 20130123, https://doi.org/10.1098/rstb.2013.0123, 2013.

Bouwman, A. F., G. Van Drecht, J. M. Knoop, A. H. W. Beusen, and C. R. Meinardi.: Exploring Changes in River Nitrogen Export to the Worlds Oceans, Global Biogeochemical Cycles, 19, GB1002, https://doi.org/10.1029/2004GB002314, 2005.

Bouwman A F , Beusen A H W , Overbeek C C , et al.: Hindcasts and Future Projections of Global Inland and Coastal Nitrogen and Phosphorus Loads Due to Finfish Aquaculture, Reviews in Fisheries Science, 21, 112-156, https://doi.org/10.1080/10641262.2013.790340, 2013.

Bouwman, A. F., Pawlowski, M., Beusen, A. H. W., et al.: Hindcasts and Future Projections of Global Inland and Coastal Nitrogen and Phosphorus Loads Due to Finfish Aquaculture, Reviews in Fisheries Science, 21, 112–56, https://doi.org/10.1080/10641262.2013.790340, 2013.

https://doi.org/10.5194/esd-2024-29
Preprint. Discussion started: 28 August 2024

971 Bu, Hongmei, Xianfang Song, and Yuan Zhang.: Using Multivariate Statistical
972 Analyses to Identify and Evaluate the Main Sources of Contamination in
973 a Polluted River near to the Liaodong Bay in Northeast China,
974 Environmental Pollution, 245, 1058–70.
975 https://doi.org/10.1016/j.envpol.2018.11.099, 2019.

976 Costa, Jéssica Alves da, João Paulo de Souza, Ana Paula Teixeira, João Carlos
977 Nabout, and Fernanda Melo Carneiro.: Eutrophication in Aquatic
978 Ecosystems. A Scientometric Study, Acta Limnologica Brasiliensia 30,
979 e2, https://doi.org/10.1590/S2179-975X3016, 2018.

980 Dai, Minhan, Yangyang Zhao, Fei Chai, Mingru Chen, Nengwang Chen, Yimin
981 Chen, Danyang Cheng, et al.: Persistent Eutrophication and Hypoxia in
982 the Coastal Oceanl Cambridge Prisms: Coastal Futures, 1, e19,
983 https://doi.org/10.1017/cft.2023.7, 2023.

984 Desmit, X., V. Thieu, G. Billen, F. Campuzano, V. Dulière, J. Garnier, L.
985 Lassaletta, et al.: Reducing Marine Eutrophication May Require a
986 Paradigmatic Change, Science of The Total Environment, 635, 1444–66.
987 https://doi.org/10.1016/j.scitotenv.2018.04.181, 2018.

988 Dodds, Walter K., and Val H. Smith.: Nitrogen, Phosphorus, and Eutrophication
989 in Streams, Inland Waters, 6, 155–64. https://doi.org/10.5268/IW-
990 6.2.909, 2016.

991 Donnelly, Chantal, Wei Yang, and Joel Dahné.: River Discharge to the Baltic
992 Sea in a Future Climate, Climatic Change 122, 157–70.
993 https://doi.org/10.1007/s10584-013-0941-y, 2014.

994 Federal Institute of Hydrology. Global river data centre. Federal Institute of
995 Hydrology, Retrieved from https://www.bafg.de/RGDC/EN/01_GRDC
996 /grdc_node.html , 2018.

997 Fekete, Balázs M., Dominik Wisser, Carolien Kroeze, Emilio Mayorga, Lex
998 Bouwman, Wilfred M. Wollheim, and Charles Vörösmarty.:Millennium
999 Ecosystem Assessment Scenario Drivers (1970–2050): Climate and
1000 Hydrological Alterations, Global Biogeochemical Cycles, 24, 1024,
1001 https://doi.org/10.1029/2009GB003593, 2010.

1002 Feng, Maoyuan, Shushi Peng, Yilong Wang, Philippe Ciais, Daniel S. Goll,
1003 Jinfeng Chang, Yunting Fang, et al.: Overestimated Nitrogen Loss from
1004 Denitrification for Natural Terrestrial Ecosystems in CMIP6 Earth
1005 System Models, Nature Communications, 14, 3065,
1006 https://doi.org/10.1038/s41467-023-38803-z, 2023.

1007 Ferreira V, Elosegi A, D. Tiegs S, von Schiller D, Young R.: Organic Matter
1008 Decomposition and Ecosystem Metabolism as Tools to Assess the

https://doi.org/10.5194/esd-2024-29
Preprint. Discussion started: 28 August 2024

1009 Functional Integrity of Streams and Rivers–A Systematic Review,Water,
1010 12, 3523. https://doi.org/10.3390/w12123523, 2020.

1011 Filoso, S., Martinelli, L.A., Williams, M.R. et al. Land use and nitrogen export
1012 in the Piracicaba River basin, Southeast Brazil, Biogeochemistry, 65,
1013 275–294, https://doi.org/10.1023/A:1026259929269, 2003.

1014 Fowler, David, Mhairi Coyle, Ute Skiba, Mark A. Sutton, J. Neil Cape, Stefan
1015 Reis, Lucy J. Sheppard, et al.: The Global Nitrogen Cycle in the Twenty-
1016 First Century, Philosophical Transactions of the Royal Society B:
1017 Biological Sciences, 368, 20130164,
1018 https://doi.org/10.1098/rstb.2013.0164, 2013.

1019 Galloway, J. N.: 8.12 - The Global Nitrogen Cycle. In Treatise on
1020 Geochemistry, edited by Heinrich D. Holland and Karl K. Turekian, 557–
1021 83. Oxford: Pergamon, https://doi.org/10.1016/B0-08-043751-6/08160-3,
1022 2003.

1023 Gao, Xinjuan, Nengwang Chen, Dan Yu, Yinqi Wu, and Bangqin Huang.:
1024 Hydrological Controls on Nitrogen (Ammonium versus Nitrate) Fluxes
1025 from River to Coast in a Subtropical Region: Observation and Modeling.
1026 Journal of Environmental Management, 213, 382–91.
1027 https://doi.org/10.1016/j.jenvman.2018.02.051, 2018.

1028 Gao, Yang, Feng Zhou, Philippe Ciais, Chiyuan Miao, Tao Yang, Yanlong Jia,
1029 Xudong Zhou, Butterbach-Bahl Klaus, Tiantian Yang, and Guirui Yu.:
1030 Human Activities Aggravate Nitrogen-Deposition Pollution to Inland
1031 Water over China, National Science Review, 7, 430–40.
1032 https://doi.org/10.1093/nsr/nwz073, 2020.

1033 Green, Pamela A., Charles J. Vörösmarty, Michel Meybeck, James N.
1034 Galloway, Bruce J. Peterson, and Elizabeth W. Boyer.: Pre-Industrial and
1035 Contemporary Fluxes of Nitrogen through Rivers: A Global Assessment
1036 Based on Typology, Biogeochemistry, 68, 71–105,
1037 https://doi.org/10.1023/B:BIOG.0000025742.82155.92, 2004.

1038 Goll, D. S., N. Vuichard, F. Maignan, A. Jornet-Puig, J. Sardans, A. Violette, S.
1039 Peng, et al.: A Representation of the Phosphorus Cycle for ORCHIDEE
1040 (Revision 4520), Geoscientific Model Development, 10, 3745–70,
1041 https://doi.org/10.5194/gmd-10-3745-2017, 2017.

1042 Goll, D. S., E. Joetzjer, M. Huang, and P. Ciais.: Low Phosphorus Availability
1043 Decreases Susceptibility of Tropical Primary Productivity to Droughts,
1044 Geophysical Research Letters, 45, 8231–40,
1045 https://doi.org/10.1029/2018GL077736, 2018.

1046 Harrison, John A., Roxane J. Maranger, Richard B. Alexander, Anne E. Giblin,
1047 Pierre-Andre Jacinthe, Emilio Mayorga, Sybil P. Seitzinger, Daniel J.

https://doi.org/10.5194/esd-2024-29
Preprint. Discussion started: 28 August 2024

Sobota, and Wilfred M. Wollheim.: The Regional and Global Significance of Nitrogen Removal in Lakes and Reservoirs, Biogeochemistry, 93, 143–57, https://doi.org/10.1007/s10533-008-9272-x, 2009.

Hashemi, Fatemeh, Jørgen E. Olesen, Tommy Dalgaard, and Christen D. Børgesen.: Review of Scenario Analyses to Reduce Agricultural Nitrogen and Phosphorus Loading to the Aquatic Environment, Science of The Total Environment, 573, 608–26. https://doi.org/10.1016/j.scitotenv.2016.08.141, 2016.

Hou, Wanli, Xi Chen, Jinhao Wu, Chong Zhang, Jianghua Yu, Jie Bai, and Tiantian Chen.: Sources and Spatiotemporal Variations of Nitrogen and Phosphorus in Liaodong Bay, China, Marine Pollution Bulletin, 185, 114191, https://doi.org/10.1016/j.marpolbul.2022.114191, 2022.

Hu, Jing, Xiaolin Liao, Lilit G. Vardanyan, Yuanyuan Huang, Kanika S. Inglett, Alan L. Wright, and K. R. Reddy.: Duration and Frequency of Drainage and Flooding Events Interactively Affect Soil Biogeochemistry and N Flux in Subtropical Peat Soils, Science of The Total Environment, 727, 138740, https://doi.org/10.1016/j.scitotenv.2020.138740, 2020

Huang, Jing, Chang-chun Xu, Bradley G. Ridoutt, Xue-chun Wang, and Pin-an Ren.: Nitrogen and Phosphorus Losses and Eutrophication Potential Associated with Fertilizer Application to Cropland in China, Journal of Cleaner Production, 159, 171–79, https://doi.org/10.1016/j.jclepro.2017.05.008, 2017.

Islam, M. J., Jang, C., Eum, J., Jung, S. min, Shin, M. S., Lee, Y., Kim, B.: The decomposition rates of organic phosphorus and organic nitrogen in river waters, Journal of Freshwater Ecology,28(2), 239–250, https://doi.org/10.1080/02705060.2012.733969, 2012.

Liu, Hongfei, Hongwei Xu, Yang Wu, Zemin Ai, Jiaoyang Zhang, Guobin Liu, and Sha Xue.: Effects of Natural Vegetation Restoration on Dissolved Organic Matter (DOM) Biodegradability and Its Temperature Sensitivity. Water Research, 191, 116792, https://doi.org/10.1016/j.watres.2020.116792, 2021.

Jung, S. P., Y. J. KIM, and H. KANG.: Denitrification Rates and Their Controlling Factors in Streams of the Han River Basin with Different Land-Use Patterns. Pedosphere, 24, 516–28, https://doi.org/10.1016/S1002-0160(14)60038-2, 2014.

Kim, Tae-Wook, Kitack Lee, Raymond G. Najjar, Hee-Dong Jeong, and Hae Jin Jeong.: Increasing N Abundance in the Northwestern Pacific Ocean Due to Atmospheric Nitrogen Deposition. Science, 334, 505–9, https://doi.org/10.1126/science.1206583, 2011.

https://doi.org/10.5194/esd-2024-29
Preprint. Discussion started: 28 August 2024

King, Sean A., James B. Heffernan, and Matthew J. Cohen.: Nutrient Flux, Uptake, and Autotrophic Limitation in Streams and Rivers. Freshwater Science, 33, 85–98, https://doi.org/10.1086/674383, 2014.

Kirkby, C. A., J. A. Kirkegaard, A. E. Richardson, L. J. Wade, C. Blanchard, and G. Batten.: Stable Soil Organic Matter: A Comparison of C:N:P:S Ratios in Australian and Other World Soils. Geoderma, 163, 197–208, https://doi.org/10.1016/j.geoderma.2011.04.010, 2011.

Krinner, G., Nicolas Viovy, Nathalie de Noblet-Ducoudré, Jérôme Ogée, Jan Polcher, Pierre Friedlingstein, Philippe Ciais, Stephen Sitch, and I. Colin Prentice.: A Dynamic Global Vegetation Model for Studies of the Coupled Atmosphere-Biosphere System. Global Biogeochemical Cycles,19, GB1015, https://doi.org/10.1029/2003GB002199, 2005.

Lacroix, Fabrice, Tatiana Ilyina, Moritz Mathis, Goulven G. Laruelle, and Pierre Regnier.: Historical Increases in Land-Derived Nutrient Inputs May Alleviate Effects of a Changing Physical Climate on the Oceanic Carbon Cycle. Global Change Biology, 27, 5491–5513, https://doi.org/10.1111/gcb.15822, 2021.

Lauerwald, R., P. Regnier, M. Camino-Serrano, B. Guenet, M. Guimberteau, A. Ducharne, J. Polcher, and P. Ciais.: ORCHILEAK (Revision 3875): A New Model Branch to Simulate Carbon Transfers along the Terrestrial–Aquatic Continuum of the Amazon Basin. Geoscientific Model Development, 10, 3821–59, https://doi.org/10.5194/gmd-10-3821-2017, 2017.

Lauerwald, Ronny, Pierre Regnier, Bertrand Guenet, Pierre Friedlingstein, and Philippe Ciais.: How Simulations of the Land Carbon Sink Are Biased by Ignoring Fluvial Carbon Transfers: A Case Study for the Amazon Basin. One Earth, 3, 226–36, https://doi.org/10.1016/j.oneear.2020.07.009, 2020.

Lee, Rosalynn Y., Sybil Seitzinger, and Emilio Mayorga. Land-Based Nutrient Loading to LMEs: A Global Watershed Perspective on Magnitudes and Sources. Environmental Development, 17, 220–29, https://doi.org/10.1016/j.envdev.2015.09.006, 2016.

Lee, Minjin, Elena Shevliakova, Charles A. Stock, Sergey Malyshev, and P. C. D. Milly.: Prominence of the Tropics in the Recent Rise of Global Nitrogen Pollution, Nature Communications, 10, 1437, https://doi.org/10.1038/s41467-019-09468-4 , 2019.

Li, Mengfan, Jing Wang, Ding Guo, Ruirui Yang, and Hua Fu.: Effect of Land Management Practices on the Concentration of Dissolved Organic Matter in Soil: A Meta-Analysis. Geoderma, 344, 74–81, https://doi.org/10.1016/j.geoderma.2019.03.004, 2019.

https://doi.org/10.5194/esd-2024-29
Preprint. Discussion started: 28 August 2024

1128 Lindström, Göran, Charlotta Pers, Jörgen Rosberg, Johan Strömqvist, and Berit
1129 Arheimer.: Development and Testing of the HYPE (Hydrological
1130 Predictions for the Environment) Water Quality Model for Different
1131 Spatial Scales. Hydrology Research, 41, 295–319,
1132 https://doi.org/10.2166/nh.2010.007, 2010.

1133 Liu, Ruimin, Qingrui Wang, Fei Xu, Cong Men, and Lijia Guo.: Impacts of
1134 Manure Application on SWAT Model Outputs in the Xiangxi River
1135 Watershed. Journal of Hydrology, 555, 479–88,
1136 https://doi.org/10.1016/j.jhydrol.2017.10.044, 2017,

1137 Liu, Zhu, Zhu Deng, Steven J. Davis, and Philippe Ciais.: Global Carbon
1138 Emissions in 2023. Nature Reviews Earth & Environment, 5, 253–54.
1139 https://doi.org/10.1038/s43017-024-00532-2, 2024.

1140 Luscz, Emily C., Anthony D. Kendall, and David W. Hyndman.: High
1141 Resolution Spatially Explicit Nutrient Source Models for the Lower
1142 Peninsula of Michigan. Journal of Great Lakes Research, 41, 618–29,
1143 https://doi.org/10.1016/j.jglr.2015.02.004, 2015.

1144 Luscz, E.C., Kendall, A.D. & Hyndman, D.W. A spatially explicit statistical
1145 model to quantify nutrient sources, pathways, and delivery at the regional
1146 scale.Biogeochemistry,133, 37–57, https://doi.org/10.1007/s10533-017-
1147 0305-1, 2017.

1148 Lutz, Brian D., Emily S. Bernhardt, Brian J. Roberts, and Patrick J.
1149 Mulholland.: Examining the Coupling of Carbon and Nitrogen Cycles in
1150 Appalachian Streams: The Role of Dissolved Organic Nitrogen. Ecology,
1151 92, 720–32, https://doi.org/10.1890/10-0899.1, 2011.

1152 Ma, Minna, Chaoqing Song, Huajun Fang, Jingbo Zhang, Jing Wei, Shurong
1153 Liu, Xiuzhi Chen, Kerou Zhang, Wenping Yuan, and Haibo Lu.:
1154 Development of a Process-Based N_2O Emission Model for Natural Forest
1155 and Grassland Ecosystems. Journal of Advances in Modeling Earth
1156 Systems, 14, e2021MS002460, https://doi.org/10.1029/2021MS002460,
1157 2022.

1158 Maranger, Roxane, Stuart E. Jones, and James B. Cotner.: Stoichiometry of
1159 Carbon, Nitrogen, and Phosphorus through the Freshwater Pipe.
1160 Limnology and Oceanography Letters, 3, 89–101,
1161 https://doi.org/10.1002/lol2.10080, 2018.

1162 Martí, Eugènia, Nancy B. Grimm, and Stuart G. Fisher.: Pre- and Post-Flood
1163 Retention Efficiency of Nitrogen in a Sonoran Desert Stream. Journal of
1164 the North American Benthological Society, 16, 805–19,
1165 https://doi.org/10.2307/1468173, 1997.

https://doi.org/10.5194/esd-2024-29
Preprint. Discussion started: 28 August 2024

1166 Marzadri, Alessandra, Giuseppe Amatulli, Daniele Tonina, Alberto Bellin,
1167 Longzhu Q. Shen, George H. Allen, and Peter A. Raymond.: Global
1168 Riverine Nitrous Oxide Emissions: The Role of Small Streams and Large
1169 Rivers. Science of The Total Environment, 776 145148,
1170 https://doi.org/10.1016/j.scitotenv.2021.145148, 2021.

1171 Mayorga, Emilio, Sybil P. Seitzinger, John A. Harrison, et al. : Global Nutrient
1172 Export from WaterSheds 2 (NEWS 2): Model Development and
1173 Implementation. Environmental Modelling & Software, 25, 837–53,
1174 https://doi.org/10.1016/j.envsoft.2010.01.007, 2010.

1175 McDowell, Rich W., Alasdair Noble, Peter Pletnyakov, and Luke M. Mosley.:
1176 Global Database of Diffuse Riverine Nitrogen and Phosphorus Loads and
1177 Yields. Geoscience Data Journal, 8, 132–43,
1178 https://doi.org/10.1002/gdj3.111, 2021.

1179 Moore, Richard B., Craig M. Johnston, Richard A. Smith, and Bryan Milstead.:
1180 Source and Delivery of Nutrients to Receiving Waters in the Northeastern
1181 and Mid-Atlantic Regions of the United States. JAWRA Journal of the
1182 American Water Resources Association, 47, 965–90,
1183 https://doi.org/10.1111/j.1752-1688.2011.00582.x, 2011.

1184 Morée, A. L., A. H. W. Beusen, A. F. Bouwman, and W. J. Willems.: Exploring
1185 Global Nitrogen and Phosphorus Flows in Urban Wastes during the
1186 Twentieth Century. Global Biogeochemical Cycles, 27, 836–46,
1187 https://doi.org/10.1002/gbc.20072, 2013.

1188 Newbold, J. D., Elwood, J. W., O'Neill, R. V., and Winkle, W. V.:
1189 Measuring nutrient spiraling in streams, Can. J. Fish. Aquat. Sci.,
1190 38, 860–863, 1981.

1191 Niu HW, Lu XX, Zhang GT, Sarangi C, Investigation of water-soluble organic
1192 constituents and their spatio-temporal heterogeneity over the Tibetan
1193 Plateau, Environmental Pollution, 302, 119093,
1194 https://doi.org/10.1016/j.envpol.2022.119093, 2022.

1195 Ngo-Duc, T., J. Polcher, and K. Laval.: A 53-Year Forcing Data Set for Land
1196 Surface Models. Journal of Geophysical Research: Atmospheres 110,
1197 D06116 ,https://doi.org/10.1029/2004JD005434, 2005.

1198 Patil M M .Interpolation Techniques in Image Resampling[J].International
1199 Journal of Engineering and Technology, 7, 567-570,
1200 https://doi.org/10.14419/ijet.v7i3.34.19383. 2018.

1201 Pisani, O., Boyer, J.N., Podgorski, D.C. et al. Molecular composition and
1202 bioavailability of dissolved organic nitrogen in a lake f Beusen low-
1203 influenced river in south Florida, USA. Aquat Sci, 79, 891–908,
1204 https://doi.org/10.1007/s00027-017-0540-5, 2017.

https://doi.org/10.5194/esd-2024-29
Preprint. Discussion started: 28 August 2024


Earth System Dynamics Discussions

1205 Raymond, Peter A., Christopher J. Zappa, David Butman, Thomas L. Bott, Jody
1206 Potter, Patrick Mulholland, Andrew E. Laursen, William H. McDowell,
1207 and Denis Newbold.: Scaling the Gas Transfer Velocity and Hydraulic
1208 Geometry in Streams and Small Rivers. Limnology and Oceanography:
1209 Fluids and Environments, 2, 41–53, https://doi.org/10.1215/21573689-
1210 1597669, 2012.

1211 Resplandy, L., A. Hogikyan, J. D. Müller, R. G. Najjar, H. W. Bange, D.
1212 Bianchi, T. Weber, et al.: A Synthesis of Global Coastal Ocean
1213 Greenhouse Gas Fluxes. Global Biogeochemical Cycles, 38,
1214 e2023GB007803, https://doi.org/10.1029/2023GB007803, 2024.

1215 Rodríguez-Cardona, Bianca M., Adam S. Wymore, Alba Argerich, Rebecca T.
1216 Barnes, Susana Bernal, E. N. Jack Brookshire, Ashley A. Coble, et al.:
1217 Shifting Stoichiometry: Long-Term Trends in Stream-Dissolved Organic
1218 Matter Reveal Altered C:N Ratios Due to History of Atmospheric Acid
1219 Deposition. Global Change Biology, 28, 98–114,
1220 https://doi.org/10.1111/gcb.15965, 2022.

1221 Roobaert, Alizée, Goulven G. Laruelle, Peter Landschützer, Nicolas Gruber, Lei
1222 Chou, and Pierre Regnier.: The Spatiotemporal Dynamics of the Sources
1223 and Sinks of CO2 in the Global Coastal Ocean. Global Biogeochemical
1224 Cycles 33, 1693–1714, https://doi.org/10.1029/2019GB006239, 2019.

1225 Sainju, Upendra M., William B. Stevens, Thecan Caesar-TonThat, Mark A.
1226 Liebig, and Jun Wang.: Net Global Warming Potential and Greenhouse
1227 Gas Intensity Influenced by Irrigation, Tillage, Crop Rotation, and
1228 Nitrogen Fertilization. Journal of Environmental Quality, 43, 777–88,
1229 https://doi.org/10.2134/jeq2013.10.0405, 2014.

1230 Saunders, D.L., and J. Kalff.: Nitrogen Retention in Wetlands, Lakes and
1231 Rivers. Hydrobiologia, 443, 205–212,
1232 https://doi.org/10.1023/A:1017506914063, 2001.

1233 Sánchez-Rodríguez, Antonio Rafael, Paul W. Hill, David R. Chadwick, and
1234 Davey L. Jones.: Typology of Extreme Flood Event Leads to Differential
1235 Impacts on Soil Functioning, Soil Biology and Biochemistry, 129, 153–
1236 68, https://doi.org/10.1016/j.soilbio.2018.11.019, 2019.

1237 Sattar, Md Abdus, Carolien Kroeze, and Maryna Strokal.: The Increasing
1238 Impact of Food Production on Nutrient Export by Rivers to the Bay of
1239 Bengal 1970–2050. Marine Pollution Bulletin, 80, 168–78,
1240 https://doi.org/10.1016/j.marpolbul.2014.01.017, 2014.

1241 Seiler, Christian, Sian Kou-Giesbrecht, Vivek K. Arora, and Joe R. Melton.:
1242 The Impact of Climate Forcing Biases and the Nitrogen Cycle on Land
1243 Carbon Balance Projections. Journal of Advances in Modeling Earth

https://doi.org/10.5194/esd-2024-29
Preprint. Discussion started: 28 August 2024

1244 Systems, 16, e2023MS003749, https://doi.org/10.1029/2023MS003749,
1245 2024.

1246 Seitzinger, S. P., J. A. Harrison, Egon Dumont, Arthur H. W. Beusen, and A. F.
1247 Bouwman.: Sources and Delivery of Carbon, Nitrogen, and Phosphorus
1248 to the Coastal Zone: An Overview of Global Nutrient Export from
1249 Watersheds (NEWS) Models and Their Application. Global
1250 Biogeochemical Cycles, 19, GB4S01,
1251 https://doi.org/10.1029/2005GB002606, 2005.

1252 Seitzinger, S. P., E. Mayorga, A. F. Bouwman, C. Kroeze, A. H. W. Beusen, G.
1253 Billen, G. Van Drecht, et al.: Global River Nutrient Export: A Scenario
1254 Analysis of Past and Future Trends, Global Biogeochemical Cycles, 24,
1255 GB0A08, https://doi.org/10.1029/2009GB003587, 2010.

1256 Sun, Y., D. S. Goll, J. Chang, P. Ciais, B. Guenet, J. Helfenstein, Y. Huang, et
1257 al.: Global Evaluation of the Nutrient-Enabled Version of the Land
1258 Surface Model ORCHIDEE-CNP v1.2 (R5986). Geoscientific Model
1259 Development, 14, 1987–2010, https://doi.org/10.5194/gmd-14-1987-
1260 2021, 2021.

1261 Swaney, Dennis P, Bongghi Hong, Chaopu Ti, Robert W Howarth, and
1262 Christoph Humborg.: Net Anthropogenic Nitrogen Inputs to Watersheds
1263 and Riverine N Export to Coastal Waters: A Brief Overview. Carbon and
1264 Nitrogen Cycles, 4, 203–11, https://doi.org/10.1016/j.cosust.2012.03.004,
1265 2012.

1266 Tian, Hanqin, Jia Yang, Chaoqun Lu, Rongting Xu, Josep G. Canadell, Robert
1267 B. Jackson, Almut Arneth, et al.: The Global N2O Model
1268 Intercomparison Project. Bulletin of the American Meteorological
1269 Society, 99, 1231–51, https://doi.org/10.1175/BAMS-D-17-0212.1, 2018.

1270 Tipping, Edward, Cayman J. Somerville, and Jörg Luster.: The C:N:P:S
1271 Stoichiometry of Soil Organic Matter. Biogeochemistry, 130, 117–31,
1272 https://doi.org/10.1007/s10533-016-0247-z, 2016.

1273 Thomas, R. Q., G. B. Bonan, and C. L. Goodale.: Insights into Mechanisms
1274 Governing Forest Carbon Response to Nitrogen Deposition: A
1275 Model–Data Comparison Using Observed Responses to Nitrogen
1276 Addition. Biogeosciences, 10, 3869–87, https://doi.org/10.5194/bg-10-
1277 3869-2013, 2013.

1278 Thornton, Peter E., Jean-François Lamarque, Nan A. Rosenbloom, and Natalie
1279 M. Mahowald.: Influence of Carbon-Nitrogen Cycle Coupling on Land
1280 Model Response to CO_2 Fertilization and Climate Variability. Global
1281 Biogeochemical Cycles, 21, GB4018,
1282 https://doi.org/10.1029/2006GB002868, 2007.

https://doi.org/10.5194/esd-2024-29
Preprint. Discussion started: 28 August 2024

Van Beek, L. P. H., Wada, Y., and Bierkens, M. F. P.: Global monthly water stress: 1. Water balance and water availability, Water Resour. Res., 47, W07517, https://doi.org/10.1029/2010wr009791 , 2011.

Van Drecht, G., A. F. Bouwman, J. Harrison, and J. M. Knoop.: Global Nitrogen and Phosphate in Urban Wastewater for the Period 1970 to 2050. Global Biogeochemical Cycles, 23, GB0A03, https://doi.org/10.1029/2009GB003458, 2009.

Vilmin, Lauriane, José M. Mogollón, Arthur H. W. Beusen, and Alexander F. Bouwman.: Forms and Subannual Variability of Nitrogen and Phosphorus Loading to Global River Networks over the 20th Century. Global and Planetary Change, 163, 67–85, https://doi.org/10.1016/j.gloplacha.2018.02.007, 2018.

Virro, H., G. Amatulli, A. Kmoch, L. Shen, and E. Uuemaa.: GRQA: Global River Water Quality Archive. Earth System Science Data, 13, 5483–5507, https://doi.org/10.5194/essd-13-5483-2021, 2021.

Vörösmarty, C. J., B. M. Fekete, M. Meybeck, and R. B. Lammers.: Geomorphometric Attributes of the Global System of Rivers at 30-Minute Spatial Resolution. Journal of Hydrology, 237,17–39, https://doi.org/10.1016/S0022-1694(00)00282-1, 2000.

Vuichard, N., P. Messina, S. Luyssaert, B. Guenet, S. Zaehle, J. Ghattas, V. Bastrikov, and P. Peylin.: Accounting for Carbon and Nitrogen Interactions in the Global Terrestrial Ecosystem Model ORCHIDEE (Trunk Version, Rev 4999): Multi-Scale Evaluation of Gross Primary Production. Geoscientific Model Development, 12, 4751–79, https://doi.org/10.5194/gmd-12-4751-2019, 2019.

Wachholz, A., J. W. Jawitz, and D. Borchardt.: From Iron Curtain to Green Belt: Shift from Heterotrophic to Autotrophic Nitrogen Retention in the Elbe River over 35 Years of Passive Restoration. Biogeosciences, 21, 3537–50, https://doi.org/10.5194/bg-21-3537-2024, 2024.

Wang, Xu, and Jing Zhang.: Watershed Hydrological Model HSPF Based on BASINS and the Uncertainty Analysis, Advanced Materials Research, 1073:1720–23, https://doi.org/10.4028/www.scientific.net/AMR.1073-1076.1720, 2015.

Wollheim, Wilfred M., Charles J. Vörösmarty, A. F. Bouwman, Pamela Green, John Harrison, Ernst Linder, Bruce J. Peterson, Sybil P. Seitzinger, and James P. M. Syvitski.: Global N Removal by Freshwater Aquatic Systems Using a Spatially Distributed, within-Basin Approach, Global Biogeochemical Cycles, 22, GB2026, https://doi.org/10.1029/2007GB002963, 2008.

https://doi.org/10.5194/esd-2024-29
Preprint. Discussion started: 28 August 2024


Earth System Dynamics Discussions Open Access EGU

Wymore, Adam S., Penny J. Johnes, Susana Bernal, E. N. Jack Brookshire, Hannah M. Fazekas, Ashley M. Helton, Alba Argerich, et al.: Gradients of Anthropogenic Nutrient Enrichment Alter N Composition and DOM Stoichiometry in Freshwater Ecosystems. Global Biogeochemical Cycles, 35, e2021GB006953, https://doi.org/10.1029/2021GB006953, 2021.

Xia, Xinghui, Ting Liu, Zhifeng Yang, Xueqing Zhang, and Zhongbo Yu.: Dissolved Organic Nitrogen Transformation in River Water: Effects of Suspended Sediment and Organic Nitrogen Concentration. Journal of Hydrology, 484, 96–104, https://doi.org/10.1016/j.jhydrol.2013.01.012, 2013.

Yang, Qichun, Hanqin Tian, Marjorie A. M. Friedrichs, Charles S. Hopkinson, Chaoqun Lu, and Raymond G. Najjar.: Increased Nitrogen Export from Eastern North America to the Atlantic Ocean Due to Climatic and Anthropogenic Changes during 1901–2008. Journal of Geophysical Research: Biogeosciences, 120, 1046–68, https://doi.org/10.1002/2014JG002763, 2015.

Yang, Fuxia, Hao Wang, Alexander F. Bouwman, Arthur H.W. Beusen, Xiaochen Liu, Junjie Wang, Zhigang Yu, and Qingzhen Yao.: Nitrogen from Agriculture and Temperature as the Major Drivers of Deoxygenation in the Central Bohai Sea. Science of The Total Environment, 893, 164614, https://doi.org/10.1016/j.scitotenv.2023.164614, 2023.

Yao, Yuanzhi, Hanqin Tian, Hao Shi, Shufen Pan, Rongting Xu, Naiqing Pan, and Josep G. Canadell.: Increased Global Nitrous Oxide Emissions from Streams and Rivers in the Anthropocene, Nature Climate Change, 10, 138–42. https://doi.org/10.1038/s41558-019-0665-8, 2020.

Yates, Christopher A., Penny J. Johnes, Alun T. Owen, Francesca L. Brailsford, Helen C. Glanville, Christopher D. Evans, Miles R. Marshall, et al.: Variation in Dissolved Organic Matter (DOM) Stoichiometry in U.K. Freshwaters: Assessing the Influence of Land Cover and Soil C:N Ratio on DOM Composition. Limnology and Oceanography, 64, 2328–40, https://doi.org/10.1002/lno.11186, 2019.

Zaehle, Sönke, Belinda E. Medlyn, Martin G. De Kauwe, Anthony P. Walker, Michael C. Dietze, Thomas Hickler, Yiqi Luo, et al.: Evaluation of 11 Terrestrial Carbon–Nitrogen Cycle Models against Observations from Two Temperate Free-Air CO2 Enrichment Studies. New Phytologist, 202, 803–22, https://doi.org/10.1111/nph.12697, 2014.

Zhang, H., R. Lauerwald, P. Regnier, P. Ciais, K. Van Oost, V. Naipal, B. Guenet, and W. Yuan.: Estimating the Lateral Transfer of Organic Carbon through the European River Network Using a Land Surface

https://doi.org/10.5194/esd-2024-29
Preprint. Discussion started: 28 August 2024

1362 Model. Earth System Dynamics, 13, 1119–44,
1363 https://doi.org/10.5194/esd-13-1119-2022, 2022.
1364 Zhang X, Tan Zou, Luis Lassaletta, Nathaniel D. Mueller, Francesco N.
1365 Tubiello, Matthew D. Lisk, Chaoqun Lu, et al.: Quantification of Global
1366 and National Nitrogen Budgets for Crop Production. Nature Food, 2,
1367 529–40, https://doi.org/10.1038/s43016-021-00318-5, 2021.